Fine color-tuning of Ir(III) tetrazolato complexes: synthesis, photophysical properties and OLED device fabrication

Nicola Monti,[a] Eleonora Previati,[a,e] Giulia Vigarani,[a] Massimo Cocchi,[b] Francesca Tinti,[b] Paolo Raiteri,[c] Stefano Zacchini,[a] Loris Giorgini,[a] Massimiliano Massi,[d] Stefano Stagni[a*], Valentina Fiorini.[a*]

a: Department of Industrial Chemistry "Toso Montanari", University of Bologna, Via Gobetti 85, 40129 Bologna, Italy.

b: Institute for Organic Synthesis and Photoreactivity, CNR, via Gobetti 101, 40129 Bologna, Italy.

c: Curtin Institute for Computation and School of Molecular and Life Sciences, Curtin University, P.O. Box U1987, Perth, WA 6845, Australia

d: Curtin Institute for Functional Molecules and Interfaces, School of Molecular and Life Science, Curtin University, Kent Street, Bentley 6102 WA, Australia.

e. Department of Applied Science and Technology -DISAT, Politecnico di Torino, Corso Duca degli Abruzzi 24, 10129 Torino, Italy.

ESI – ELECTRONIC SUPPLEMENTARY INFORMATION

Index

NMR spectroscopy

Figure S1: [Ir(ppyCN)$_2$(PTZ)] ^{1}H-NMR, Acetone-d^6, 400 MHz, 298K.

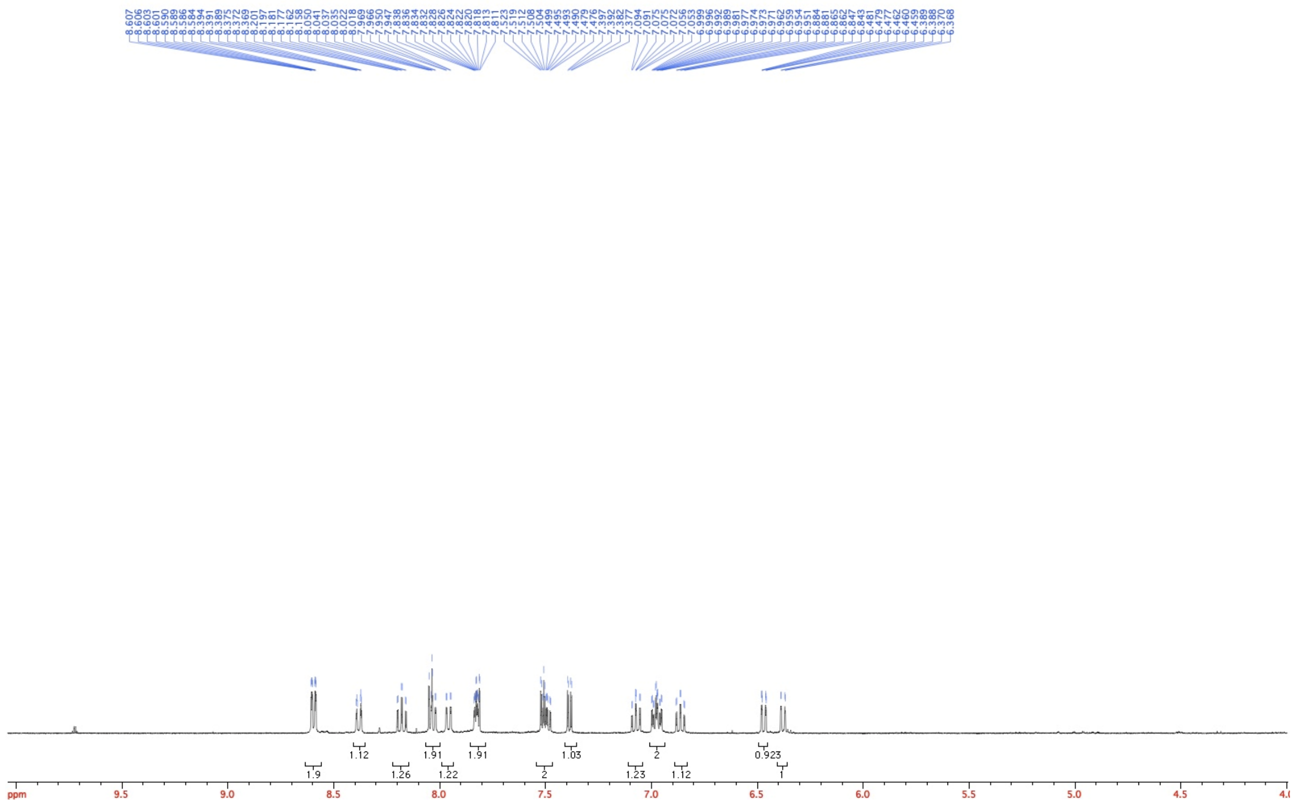

Figure S2: [Ir(ppyCN)$_2$(PTZ)] ^{13}C-NMR, Acetone-d^6, 100 MHz, 298K.

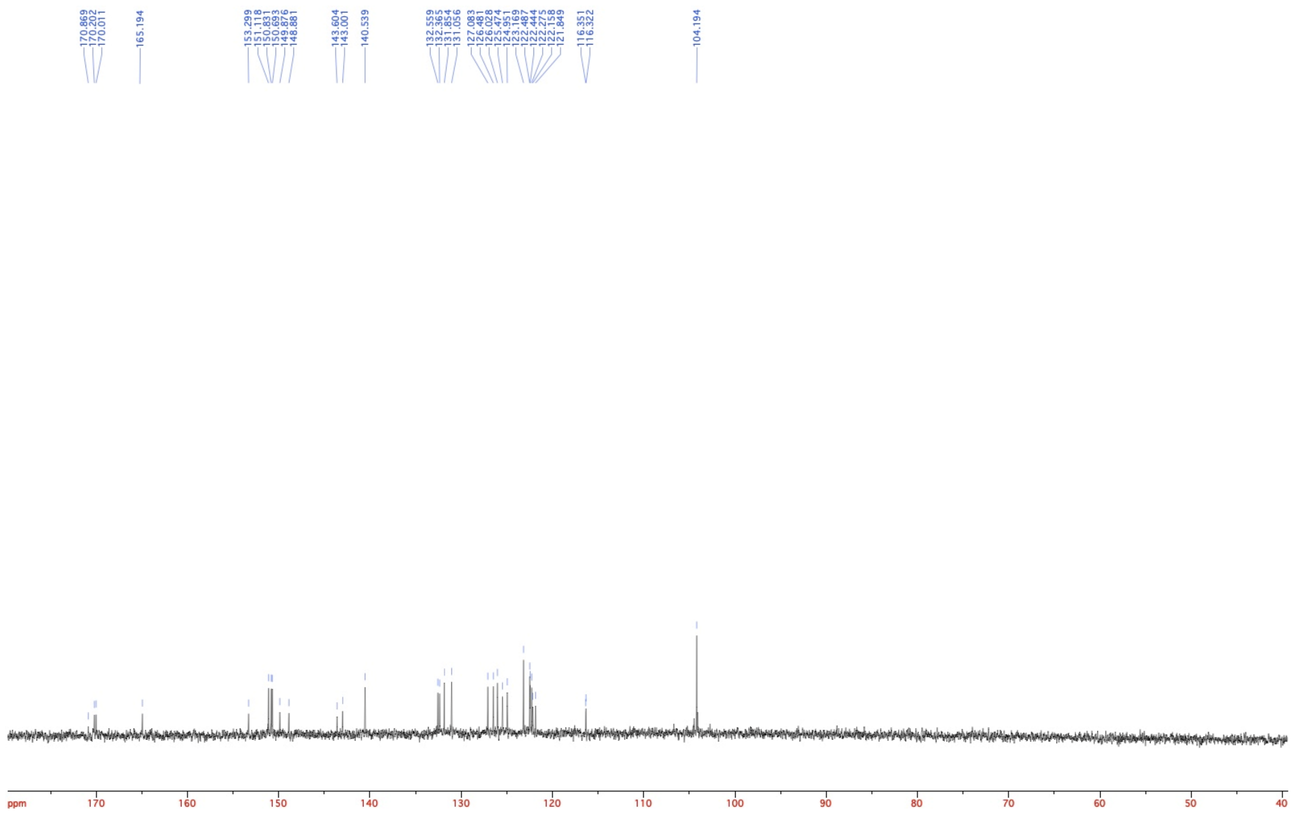

Figure S3: [Ir(ppyCN)$_2$(PYZ)] ^{1}H-NMR, Acetone-d^6, 400 MHz, 298K.

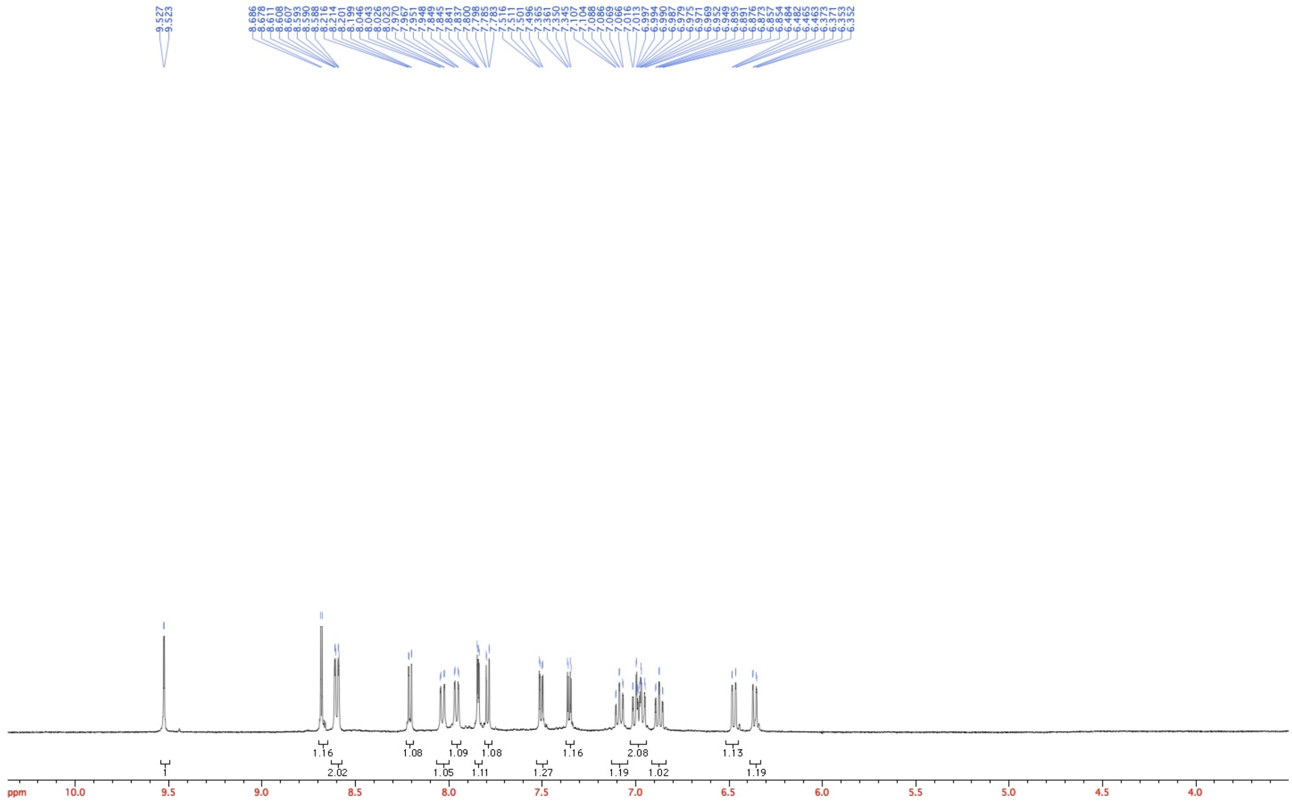

Figure S4: [Ir(ppyCN)$_2$(PYZ)] ^{13}C-NMR, CD_3CN, 100 MHz, 298K.

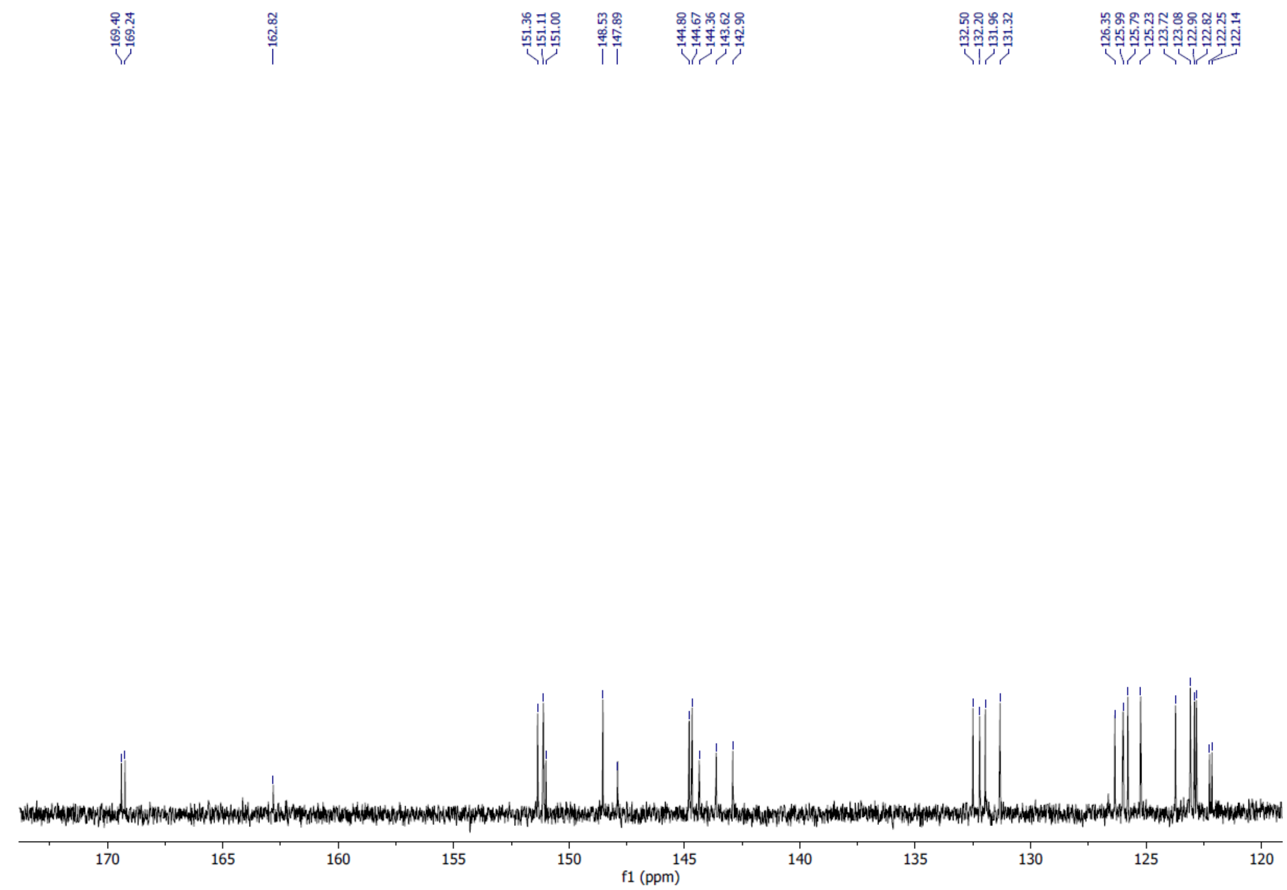

Figure S5: [Ir(ppyCN)$_2$(PTZ-CF$_3$)] ^{1}H-NMR, Acetone-d^6, 400 MHz, 298K.

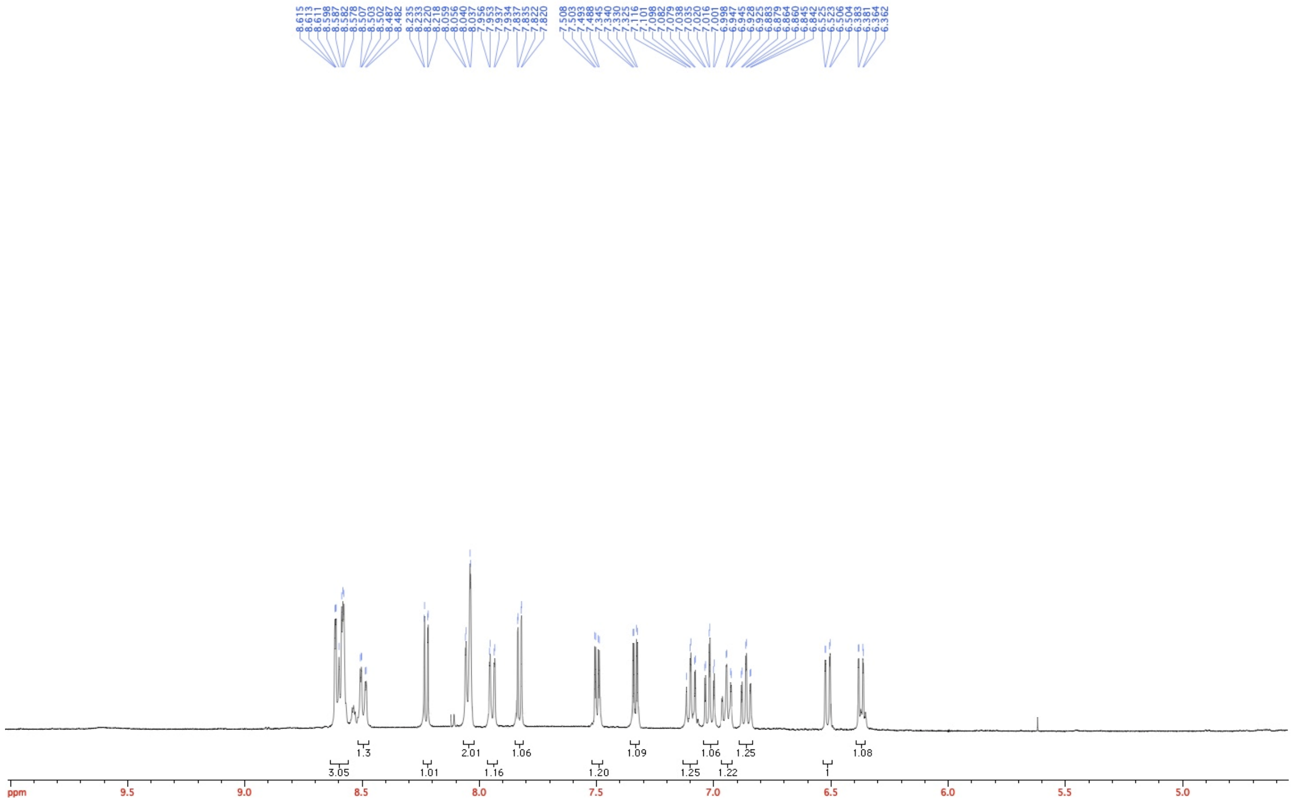

Figure S6: [Ir(ppyCN)$_2$(PTZ-CF$_3$)] ^{13}C-NMR, Acetone-d^6, 100 MHz, 298K.

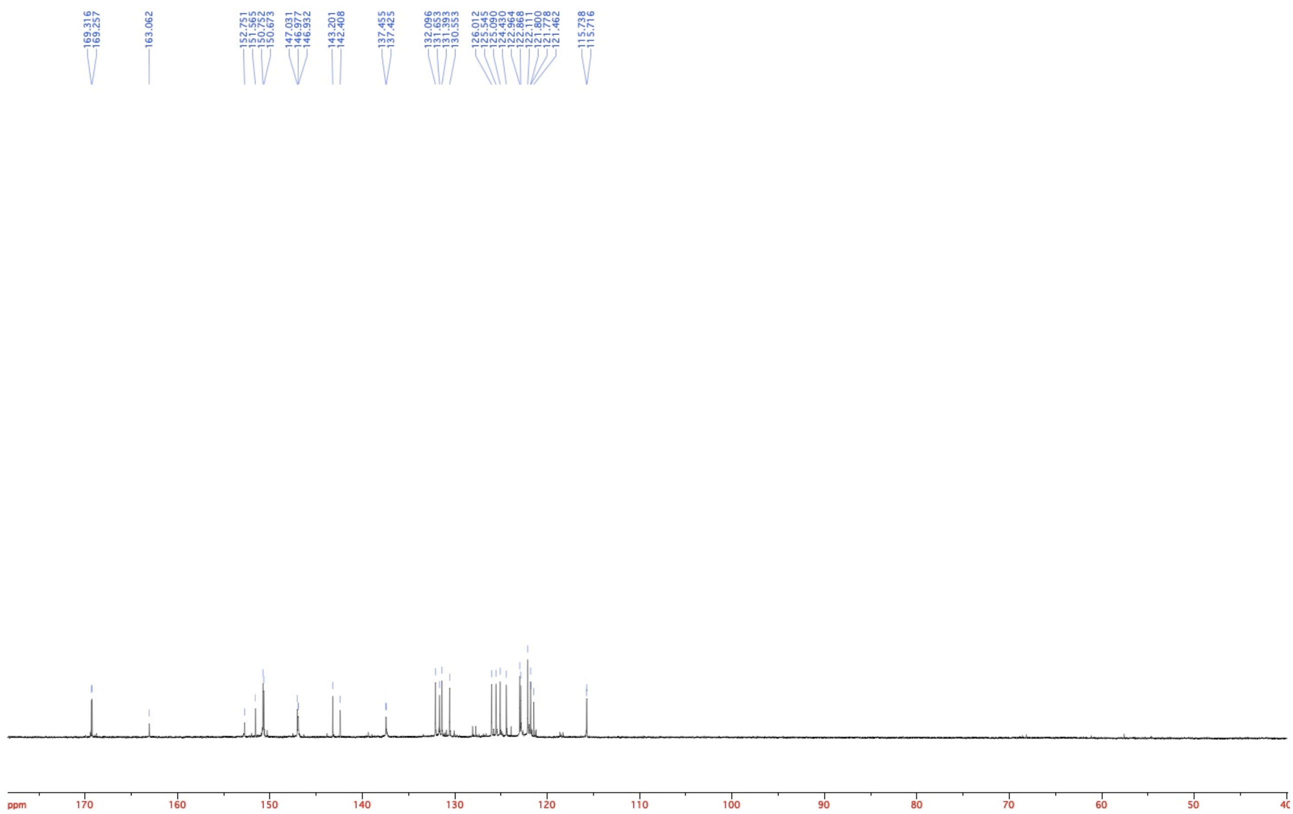

Figure S7: [Ir(F$_2$ppy-CN)$_2$(PTZ)] ^{1}H-NMR, CD_3CN, 400 MHz, 298K.

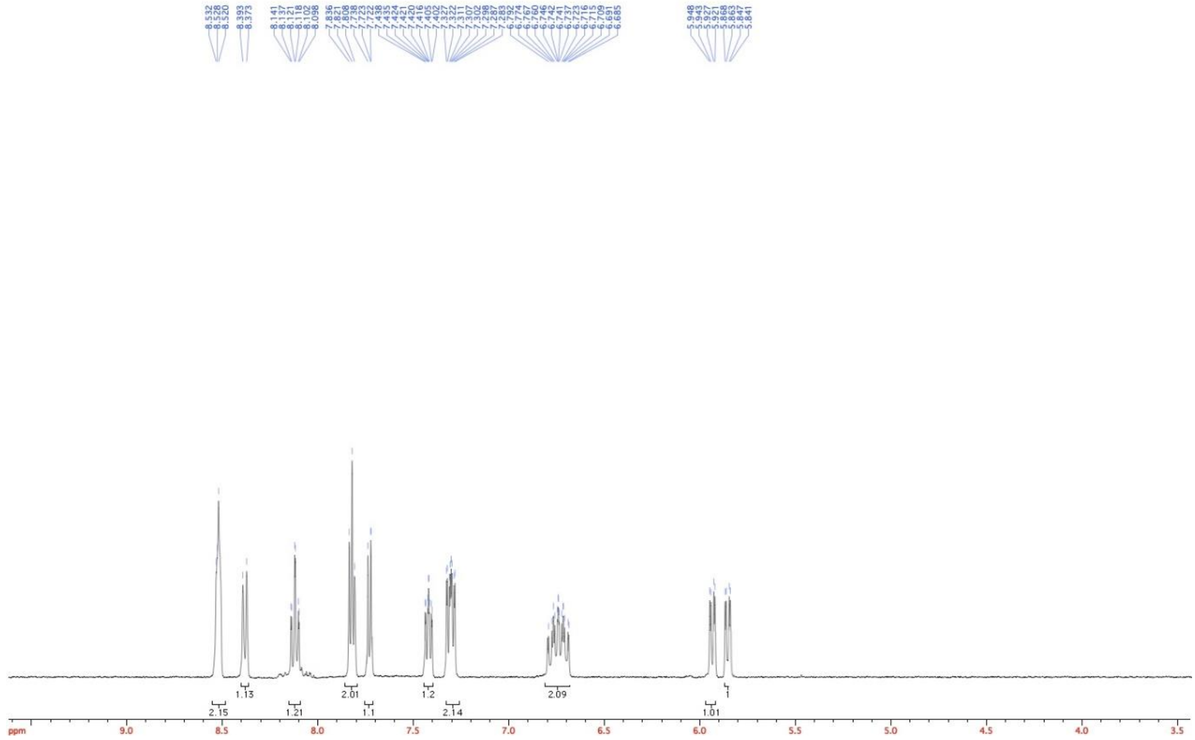

Figure S8: [Ir(F$_2$ppy-CN)$_2$ (PTZ)] ^{13}C-NMR, Acetone-d^6, 100 MHz, 298K.

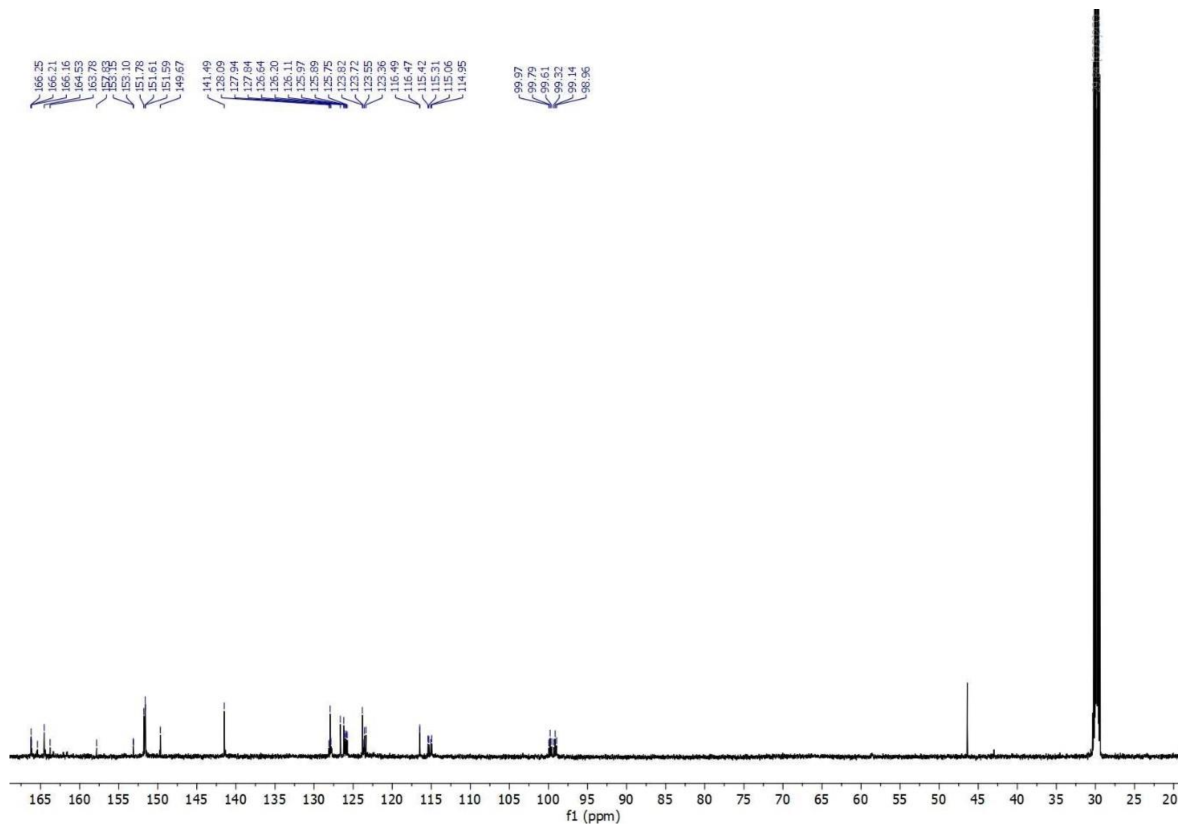

Figure S9: [Ir(F_2ppy-CN)$_2$ (PYZ)] ^{1}H-NMR, Acetone-d^6, 400 MHz, 298K.

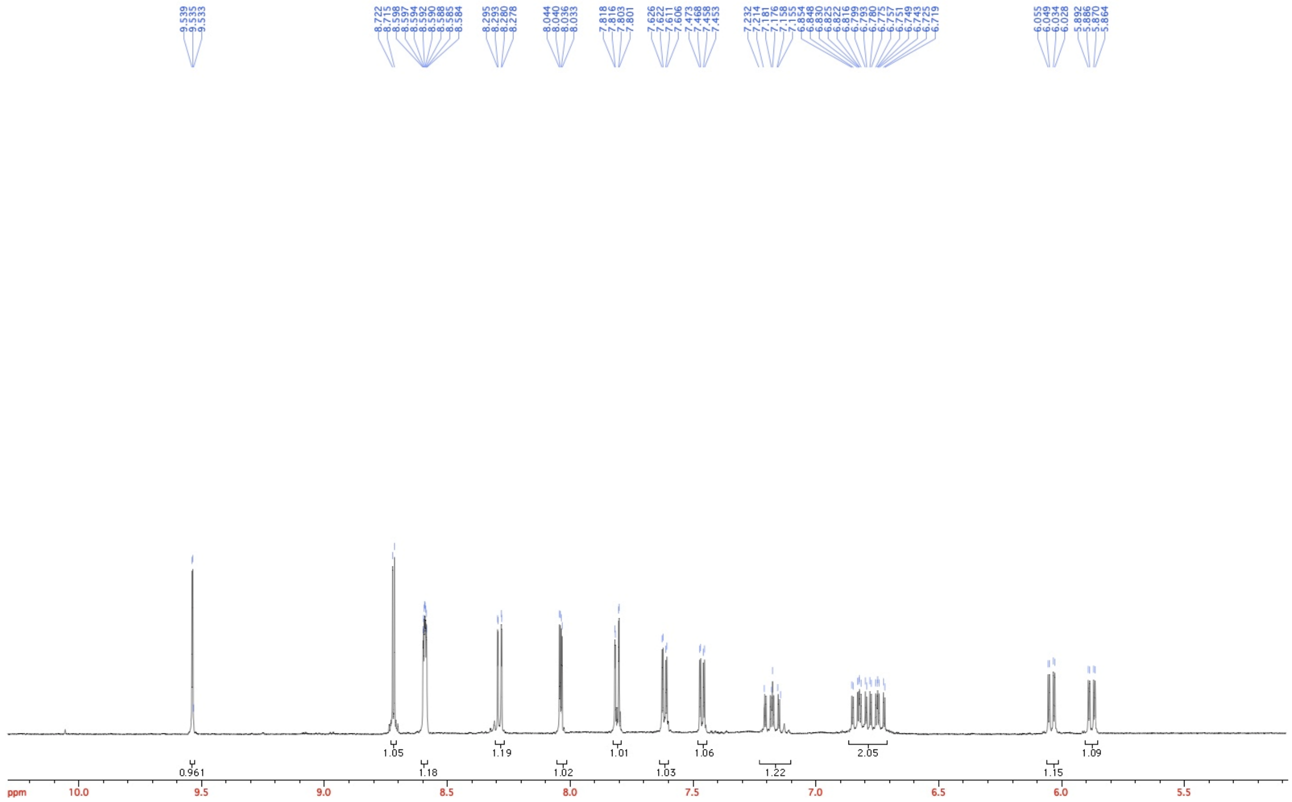

Figure S10: [Ir(F_2ppy-CN)$_2$(PYZ)] ^{13}C-NMR, Acetone-d^6, 100 MHz, 298K.

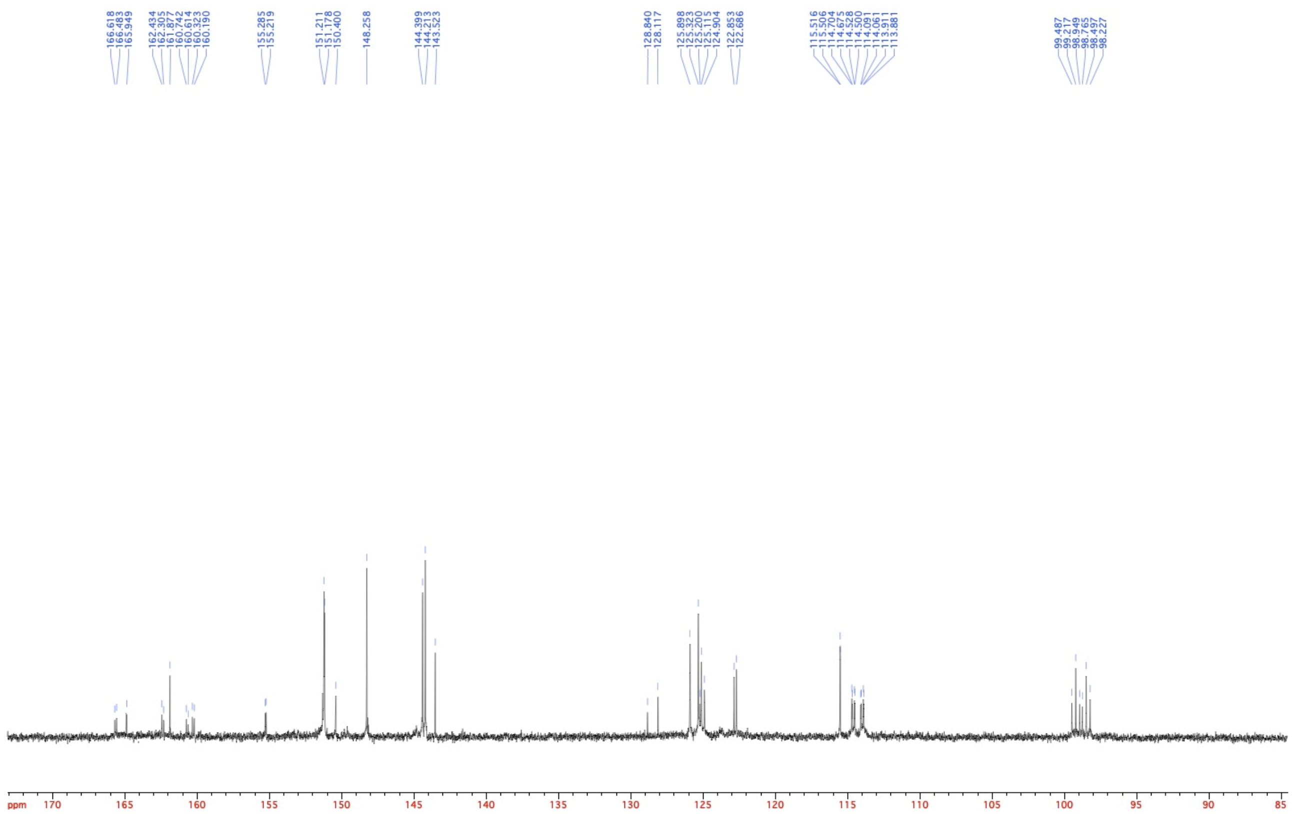

Figure S11: [Ir(F_2ppy-CN)$_2$ (PTZ-CF_3)] ^{1}H-NMR, Acetone-d^6, 400 MHz, 298K.

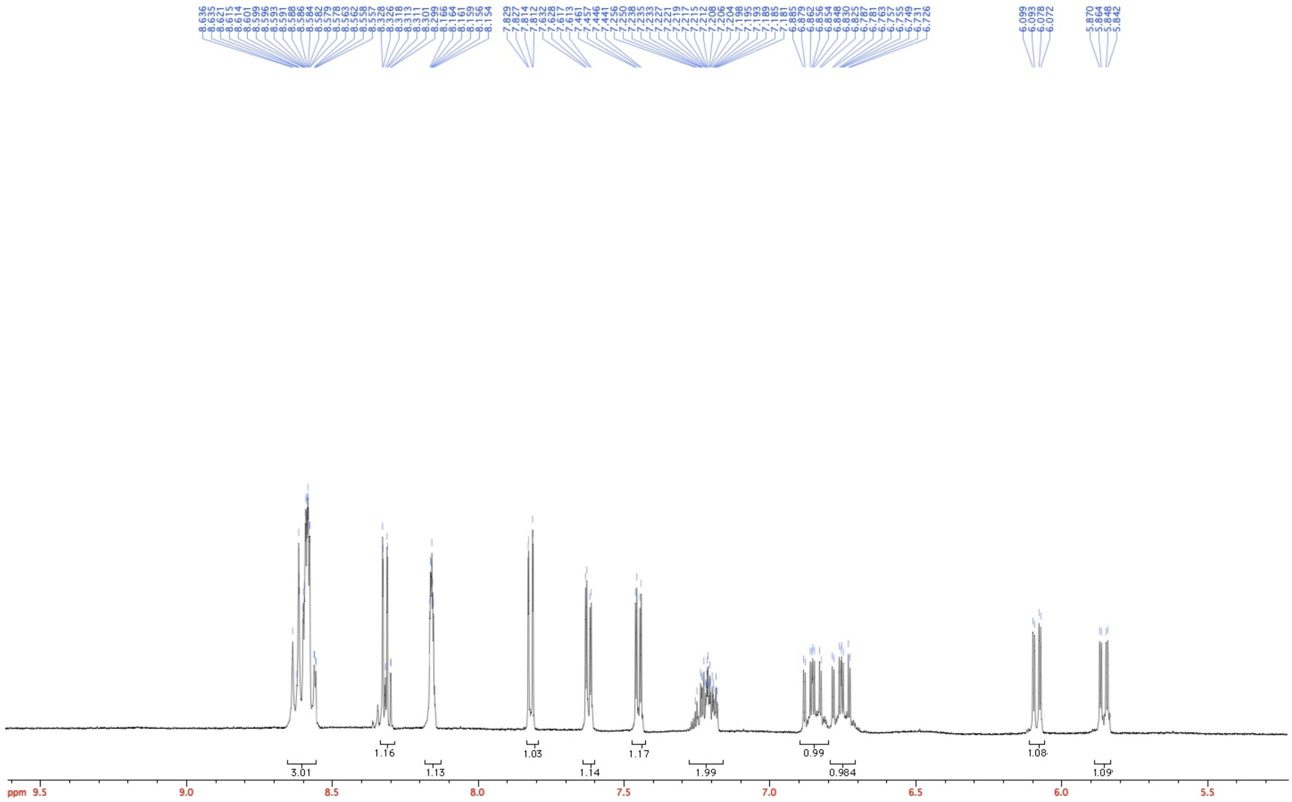

Figure S12: [Ir(F_2ppy-CN)$_2$ (PTZ-CF_3)] ^{13}C-NMR, Acetone-d^6, 100 MHz, 298K.

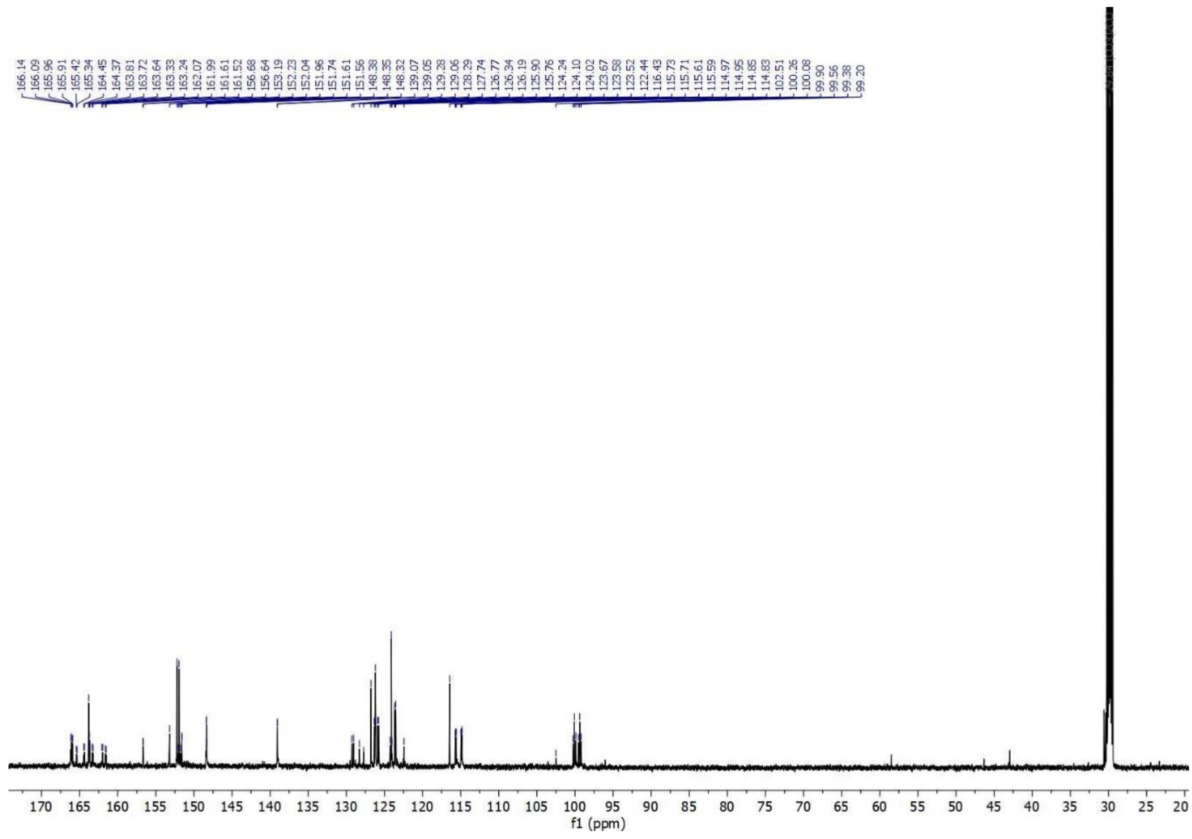

Figure S13: [Ir(ppyCN)$_2$(PTZ-Me)]$^+$[PF$_6$]$^-$ ^{1}H-NMR, Acetone-d^6, 400 MHz, 298K.

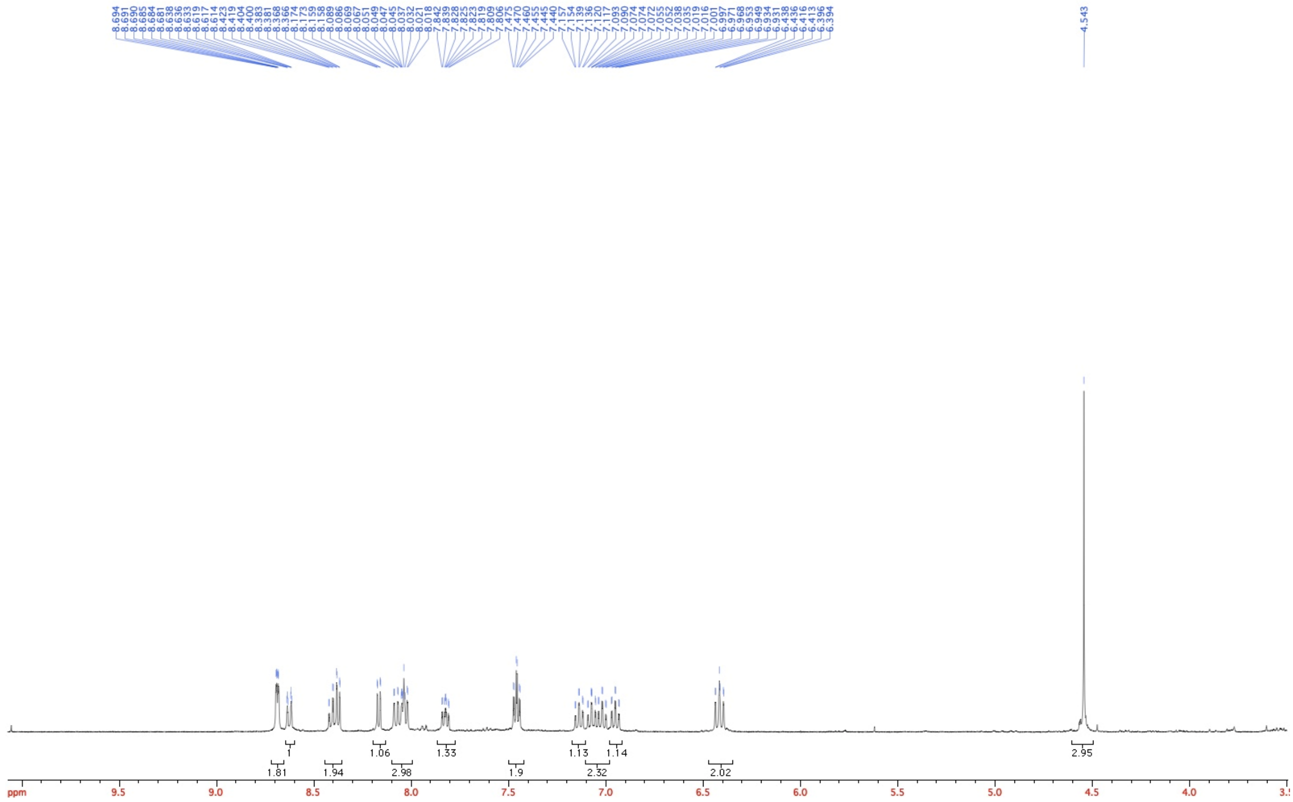

Figure S14: [Ir(ppyCN)$_2$(PTZ-Me)]$^+$[PF$_6$]$^-$ ^{13}C-NMR, Acetone-d^6, 100 MHz, 298K.

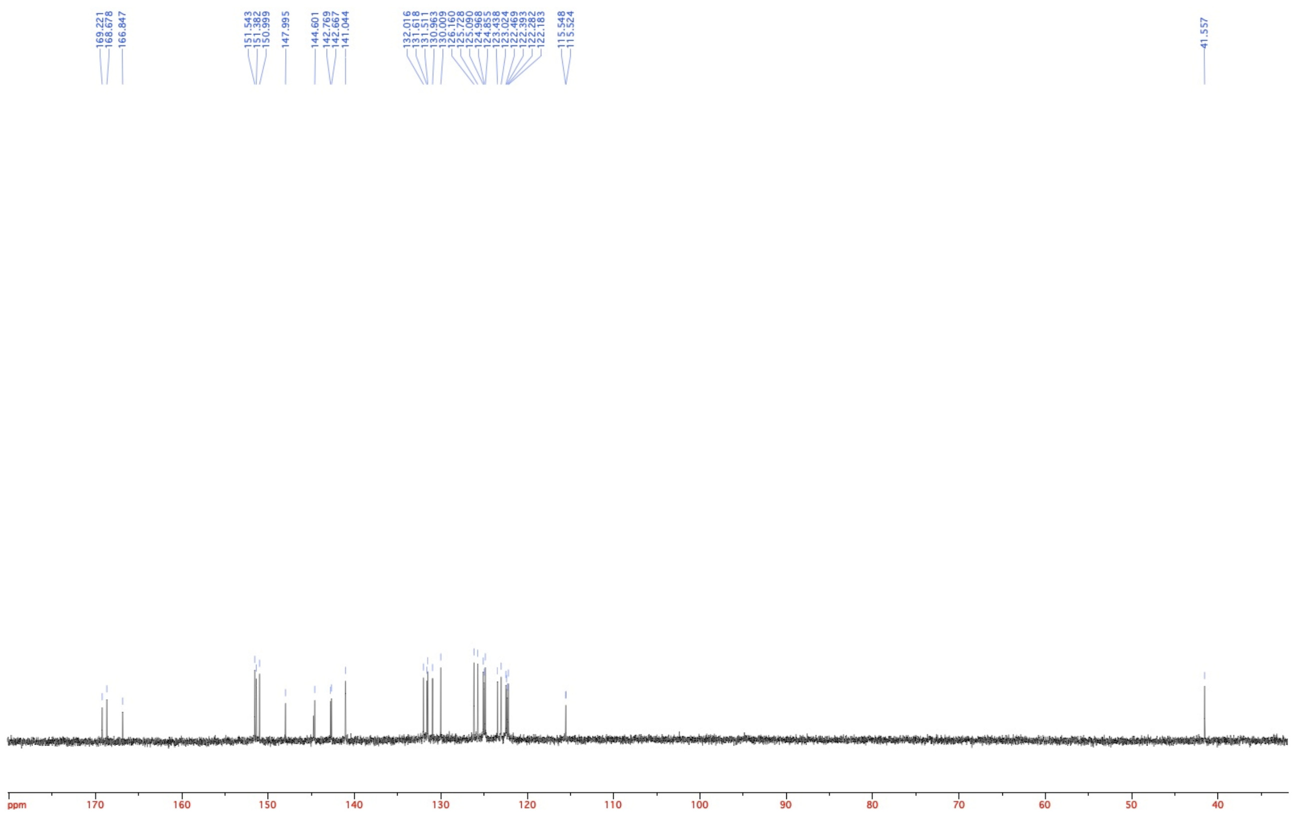

Figure S15: [Ir(ppyCN)$_2$(PYZ-Me)]$^+$[PF$_6$]$^-$ ^{1}H-NMR, Acetone-d^6, 400 MHz, 298K.

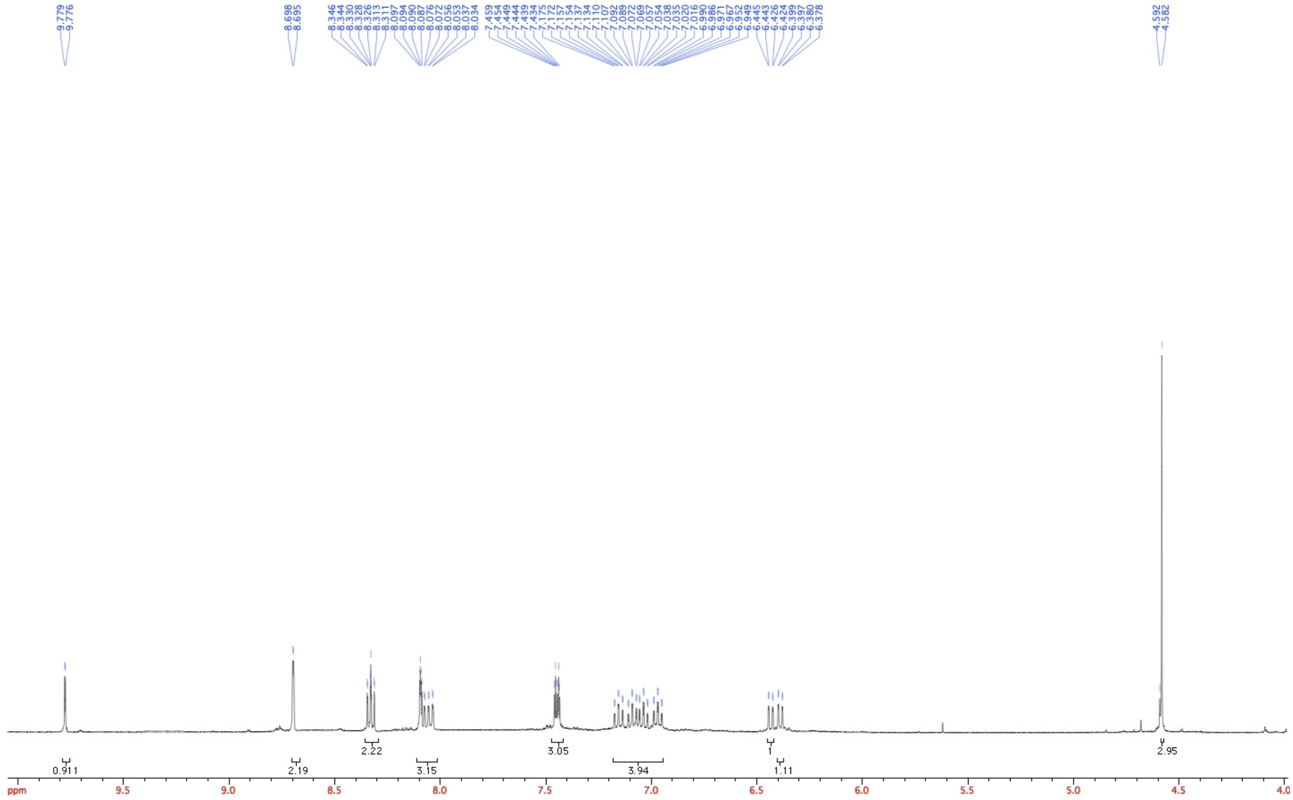

Figure S16: [Ir(ppyCN)$_2$(PYZ-Me)]$^+$[PF$_6$]$^-$ ^{13}C-NMR, Acetone-d^6, 100 MHz, 298K.

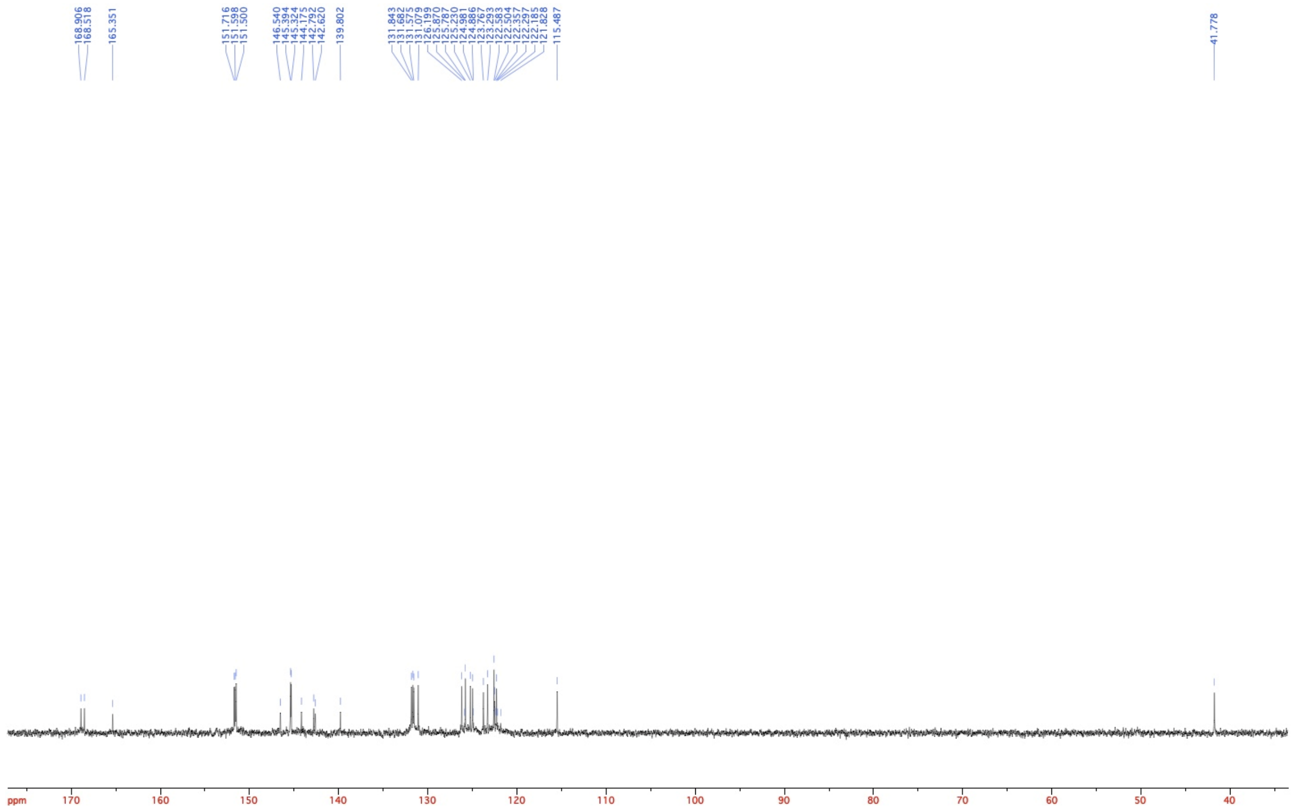

Figure S17: [Ir(ppyCN)$_2$(PTZ-CF$_3$-Me)]$^+$[PF$_6$]$^-$ ^{1}H-NMR, Acetone-d^6, 400 MHz, 298K.

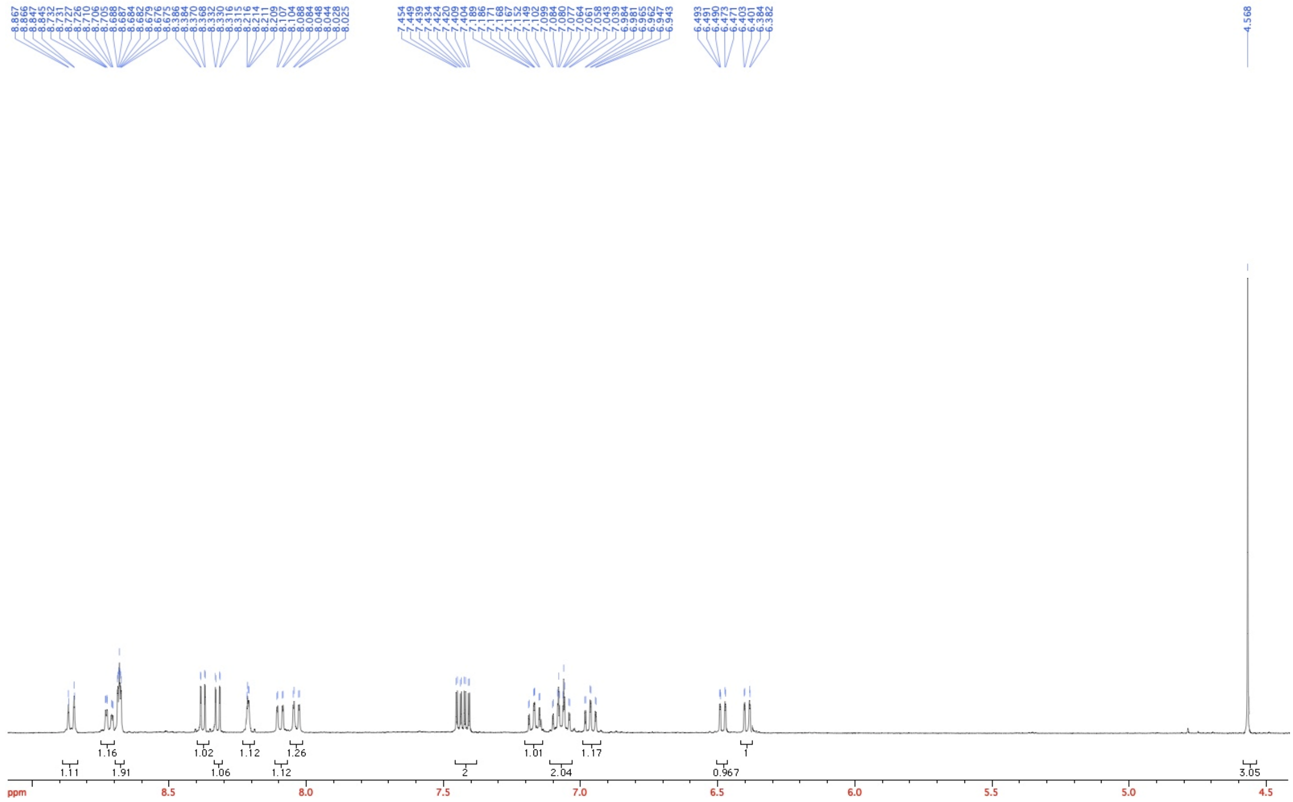

Figure S18: [Ir(ppyCN)$_2$(PTZ-CF$_3$-Me)]$^+$[PF$_6$]$^-$ ^{13}C-NMR, Acetone-d^6, 100 MHz, 298K.

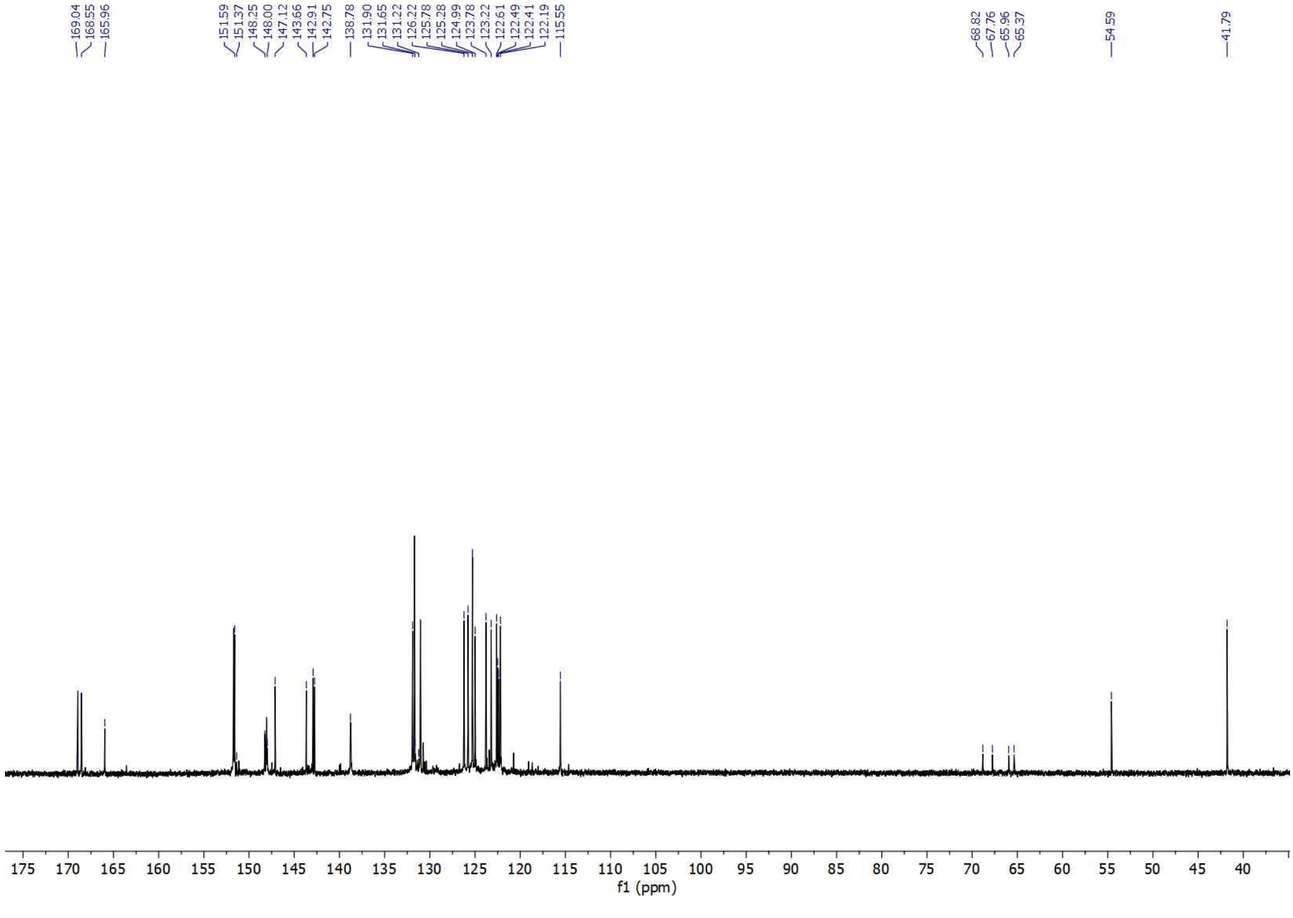

Figure S19: [Ir(F$_2$ppy-CN)$_2$(PTZ-Me)]$^+$[PF$_6$]$^-$ ^{1}H-NMR, Acetone-d^6, 400 MHz, 298K.

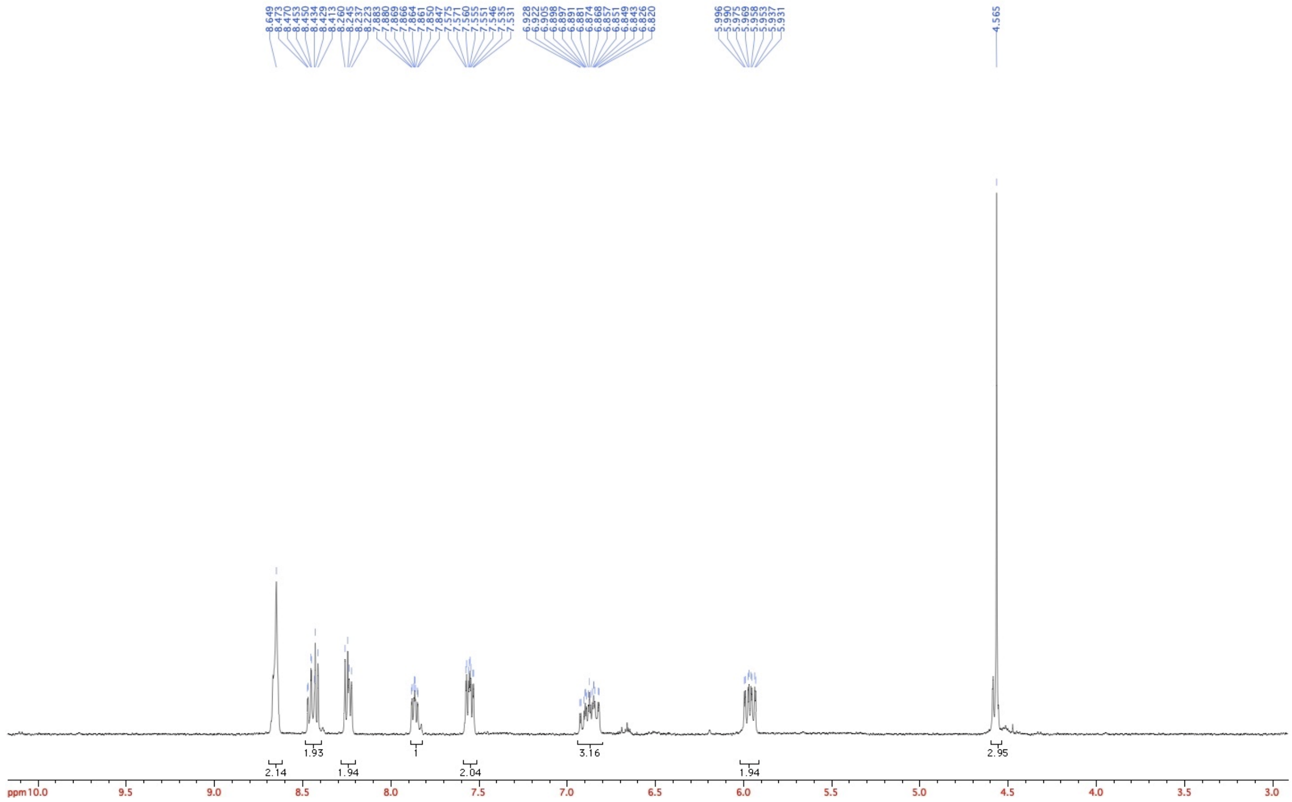

Figure S20: [Ir(F$_2$ppy-CN)$_2$(PTZ-Me)]$^+$[PF$_6$]$^-$ ^{13}C-NMR Acetone-d^6, 100 MHz, 298K.

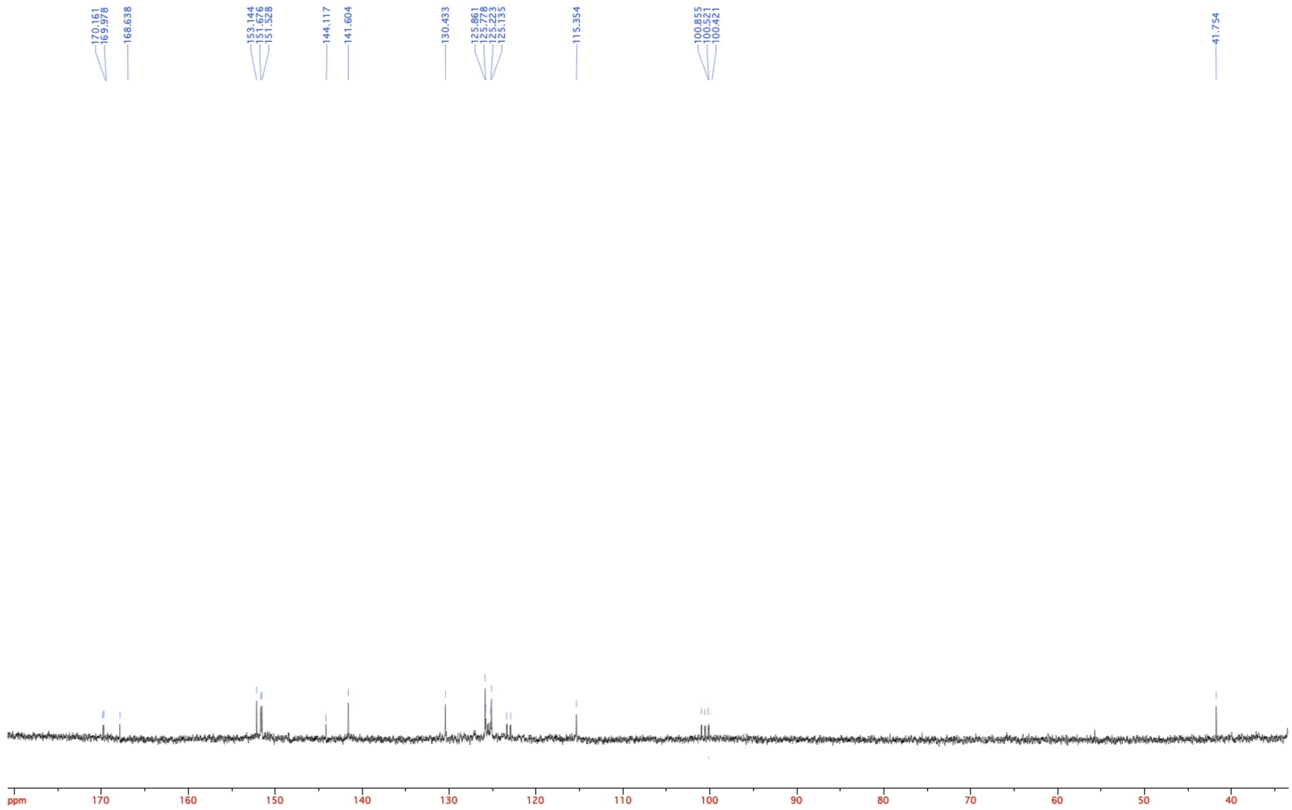

Figure S21: [Ir(F$_2$ppy-CN)$_2$(PYZ-Me)]$^+$[PF$_6$]$^-$ ^{1}H-NMR, CD$_3$CN, 400 MHz, 298K.

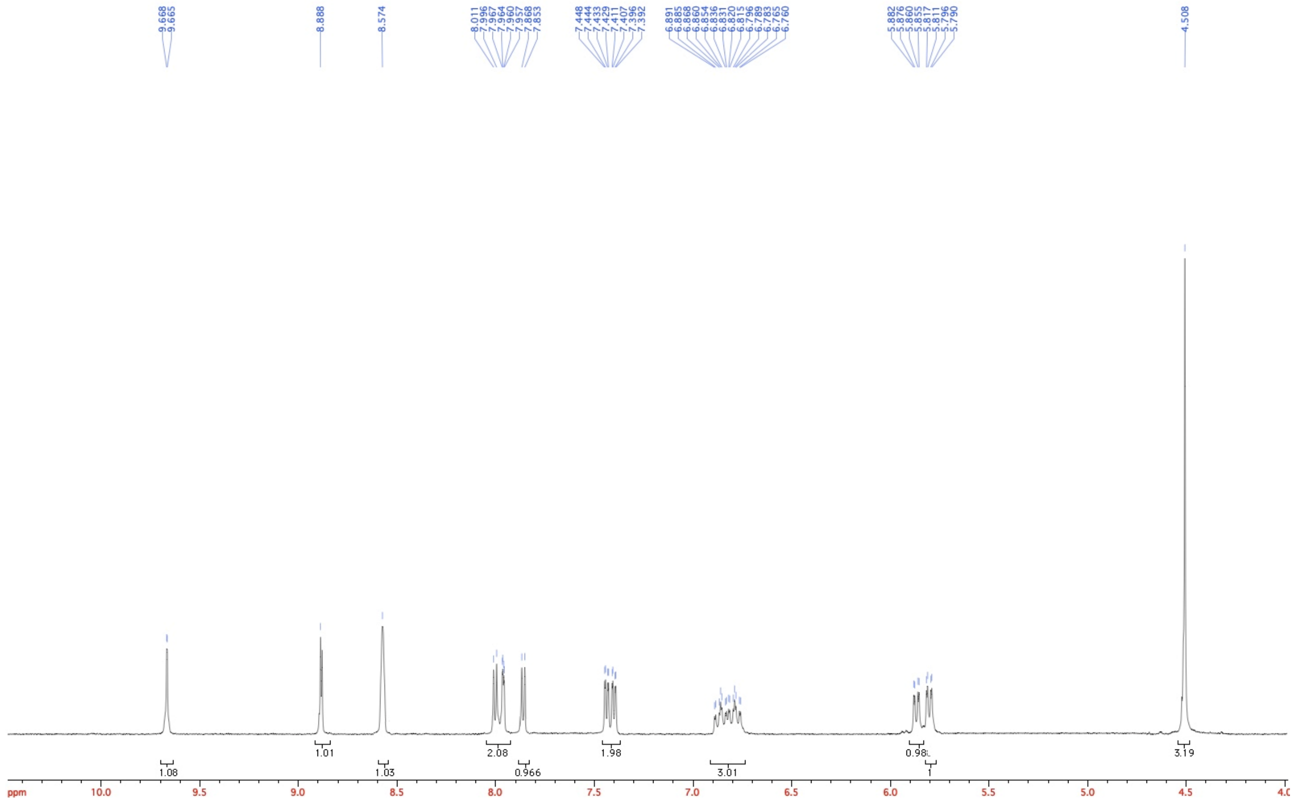

Figure S22: [Ir(F$_2$ppy-CN)$_2$(PYZ-Me)]$^+$[PF$_6$]$^-$ ^{13}C-NMR, Acetone-d^6, 100 MHz, 298K.

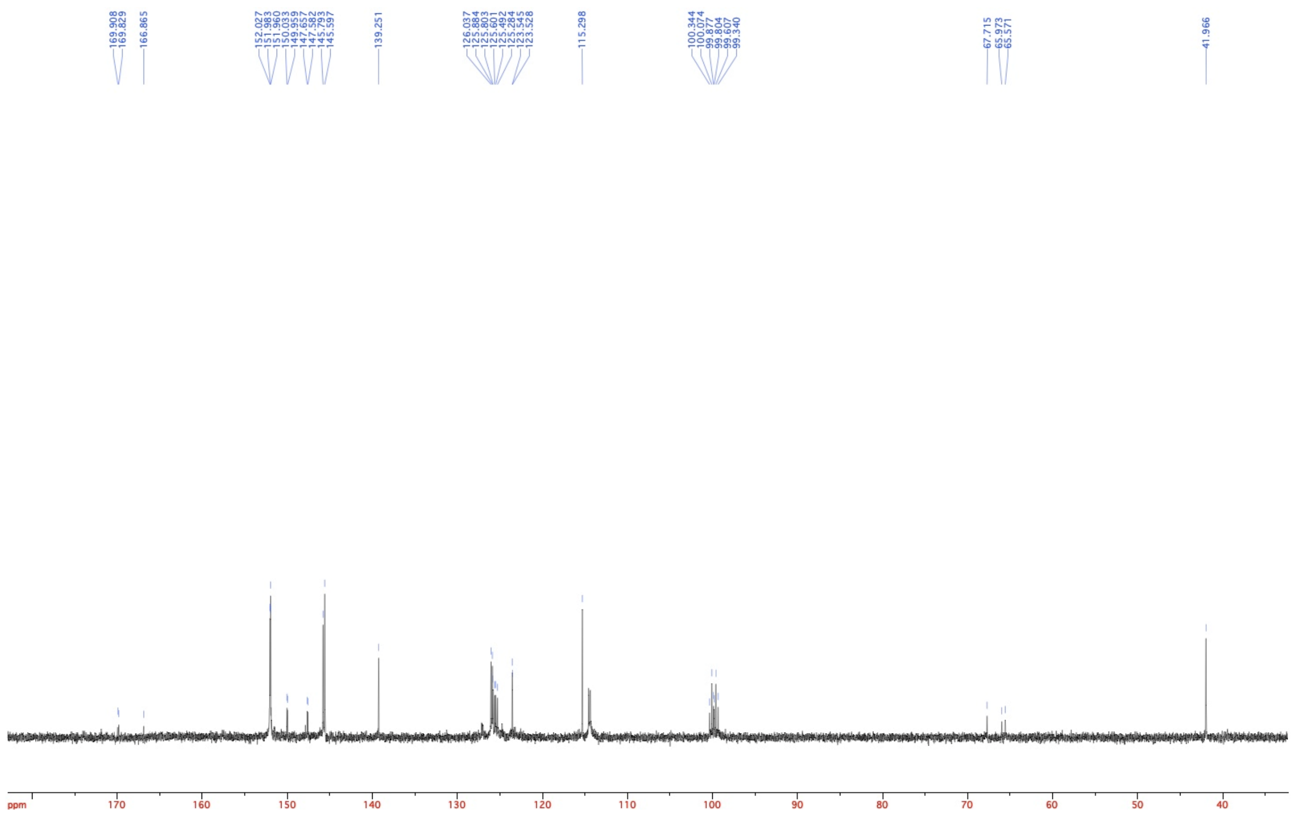

Figure S23: [Ir(F_2ppy-CN)$_2$(PTZ-CF_3-Me)]$^+$[PF_6]$^-$ ^{1}H-NMR, Acetone-d^6, 400 MHz, 298K.

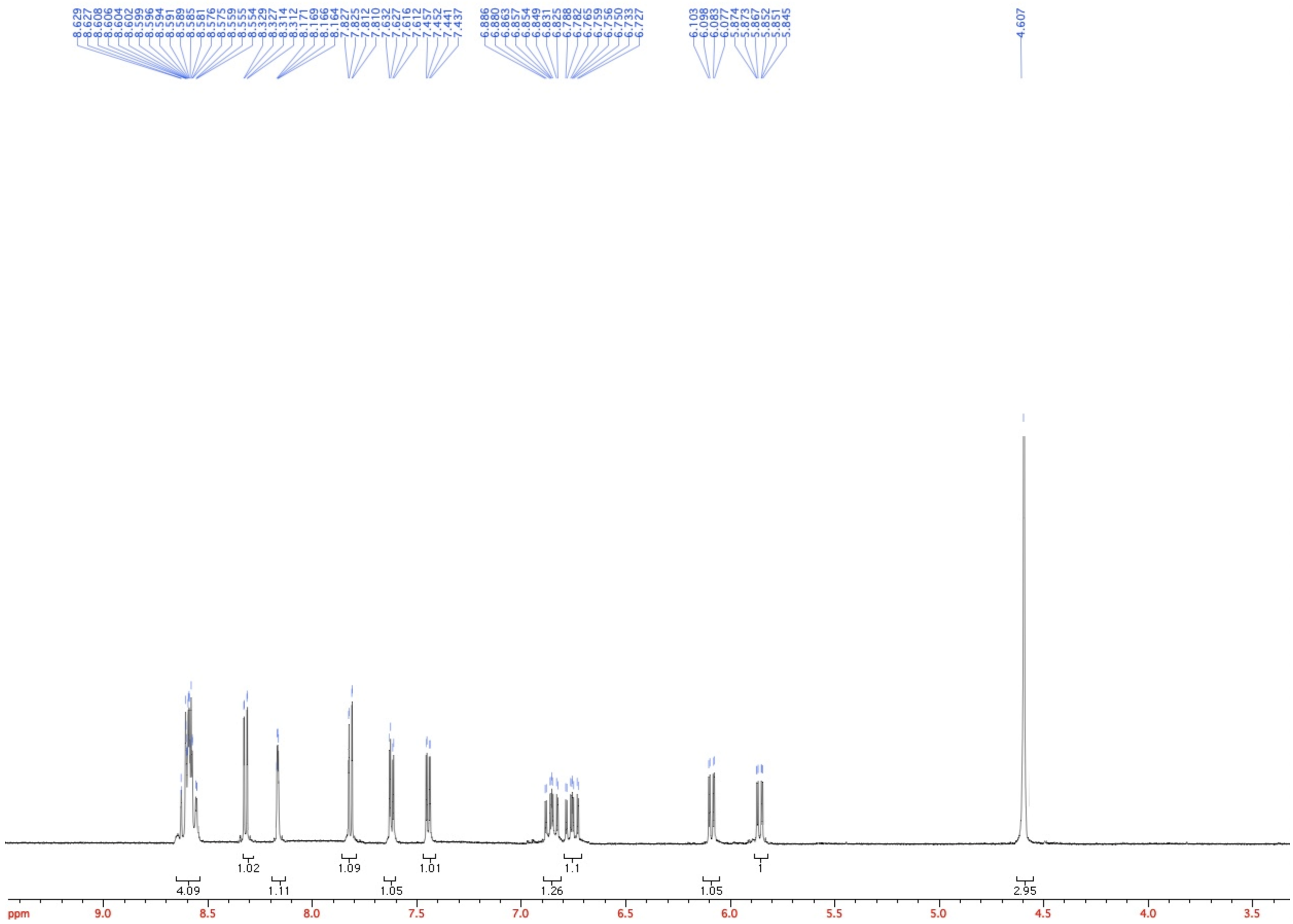

Figure S24: [Ir(F_2ppy-CN)$_2$(PTZ-CF_3-Me)]$^+$[PF_6]$^-$ ^{13}C-NMR, Acetone-d^6, 100 MHz, 298K.

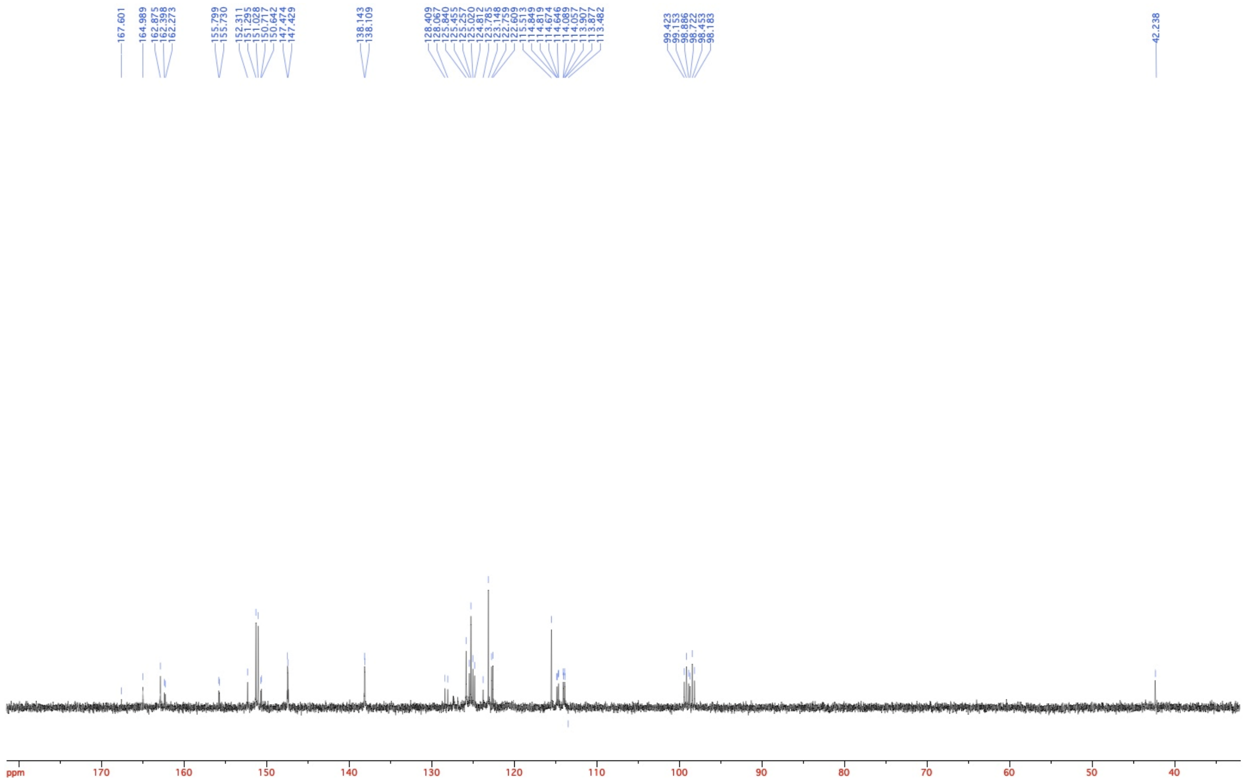

Photophysical Properties

Figure S25: Photophysical Characterization of **[Ir(ppyCN)$_2$(PTZ)]**, 10^{-5}M, CH_3CN

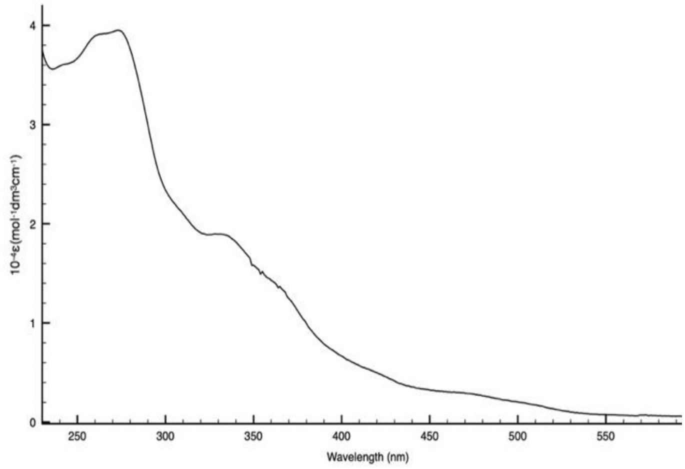

Absorption profile, 298K

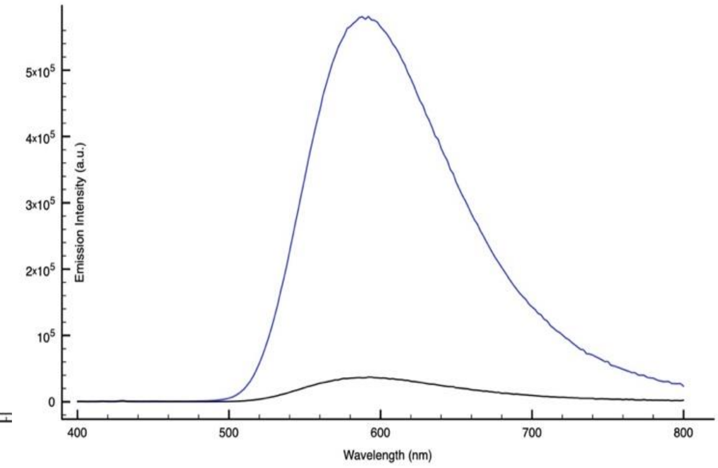

Air-equilibrated (black line) and deoxygenated (blue line) emission profiles, 298K

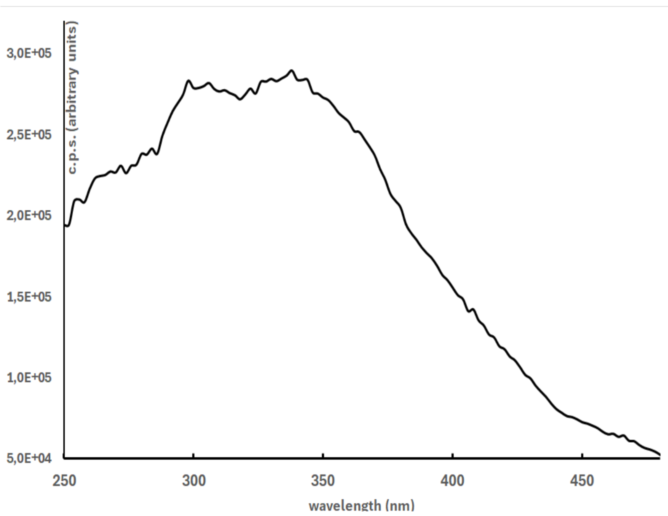

Excitation spectrum (λ_{max} = 590 nm), 298K

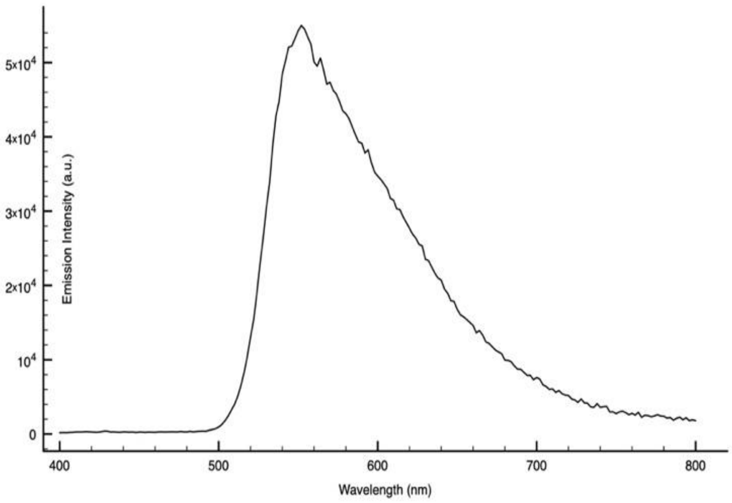

Emission profile, 77K

Figure S26: Photophysical Characterization of **[Ir(ppyCN)$_2$(PYZ)]**, 10^{-5}M, CH_3CN

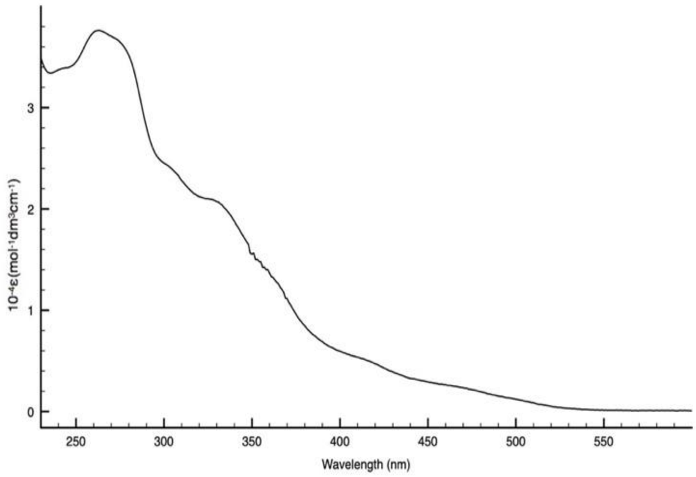

Absorption profile, 298K

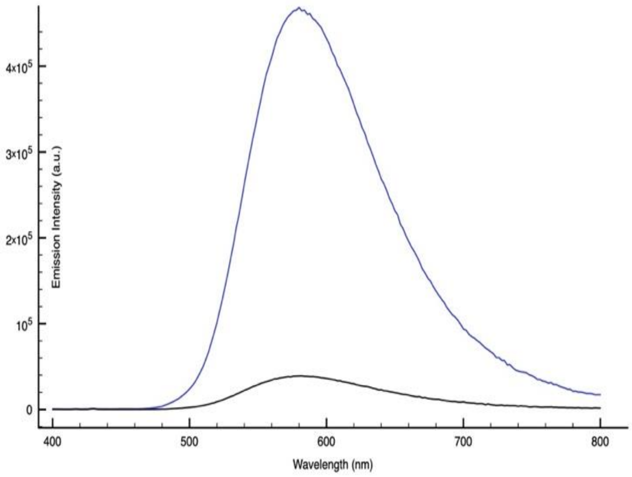

Air-equilibrated (black line) and deoxygenated (blue line) emission profiles, 298K

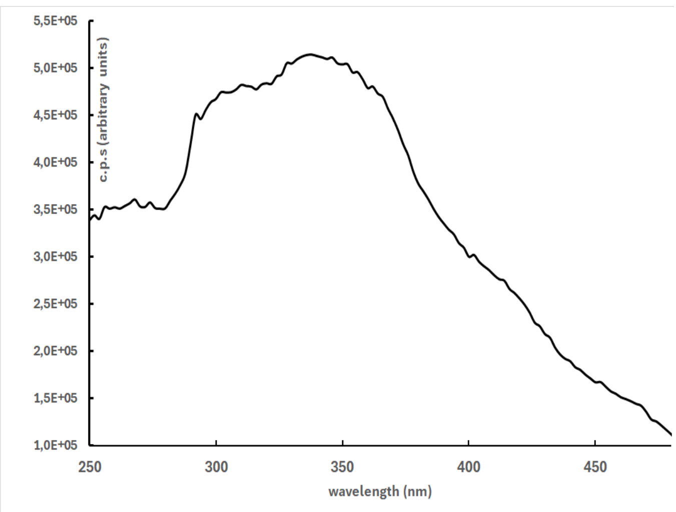

Excitation spectrum (λ_{max} = 582 nm), 298K

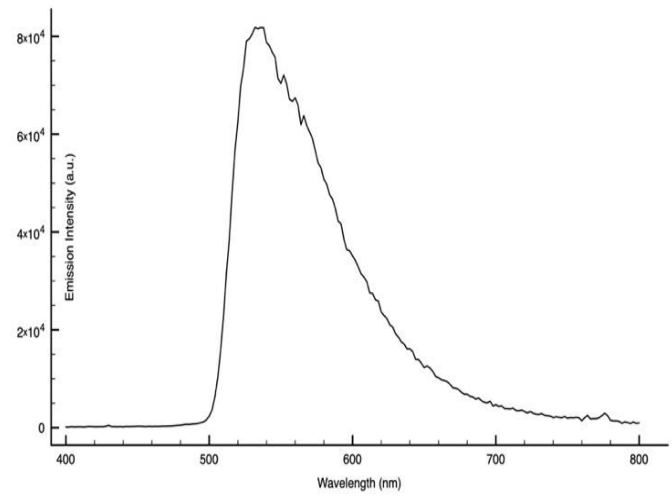

Emission profile, 77K

Figure S27: Photophysical Characterization of **[Ir(ppyCN)$_2$(PTZ-CF$_3$)]**,10^{-5}M, CH_3CN.

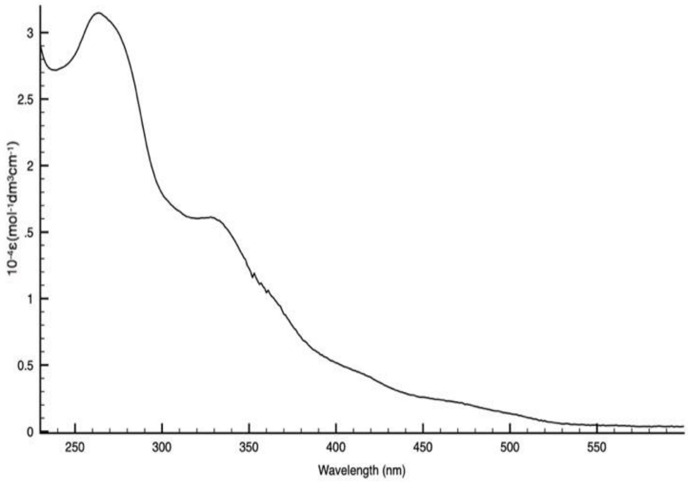

Absorption profile, 298K

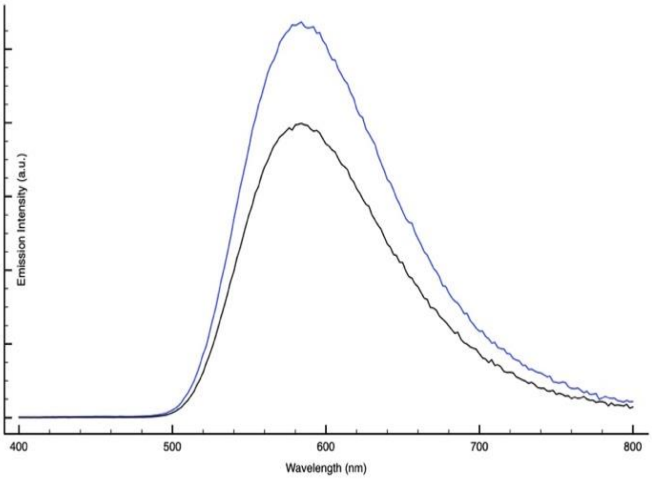

Air-equilibrated (black line) and deoxygenated (blue line) emission profiles, 298K

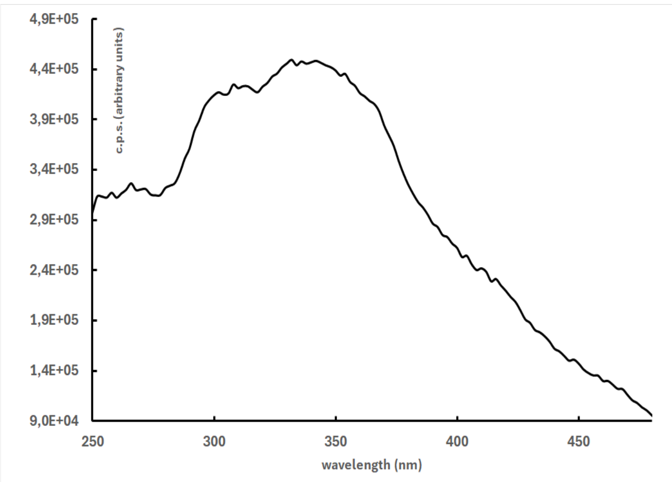

Excitation spectrum (λ_{max} = 584 nm), 298K

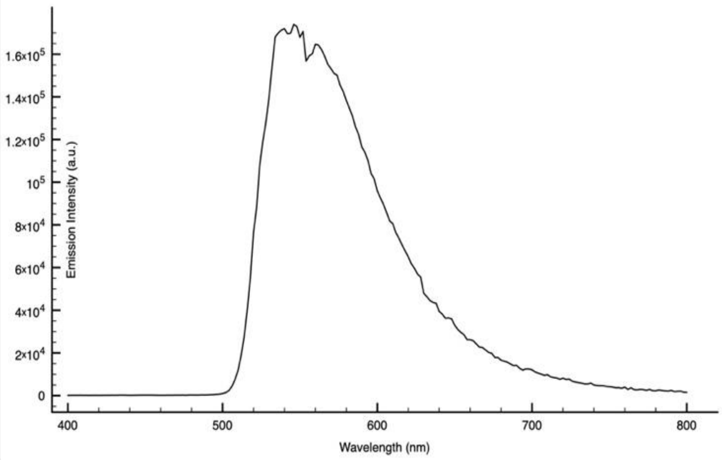

Emission profile, 77K

Figure S28: Photophysical Characterization of **$[Ir(ppyCN)_2(PTZ\text{-}Me)]^+$**, 10^{-5}M, CH_3CN.

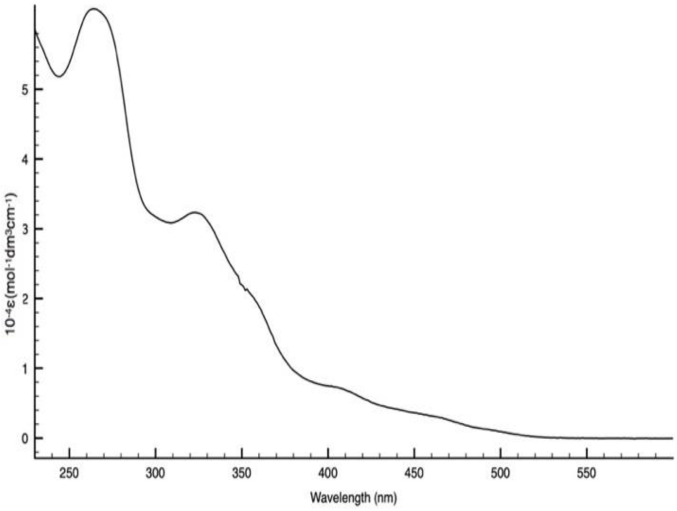

Absorption profile, 298K

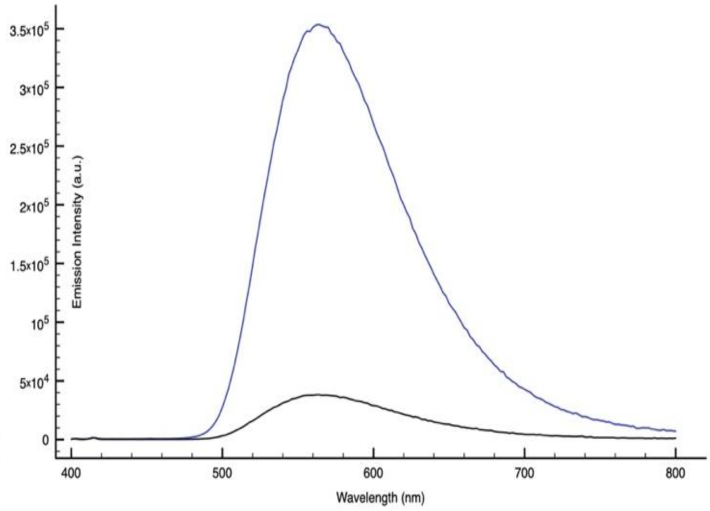

Air-equilibrated (black line) and deoxygenated (blue line) emission profiles, 298K

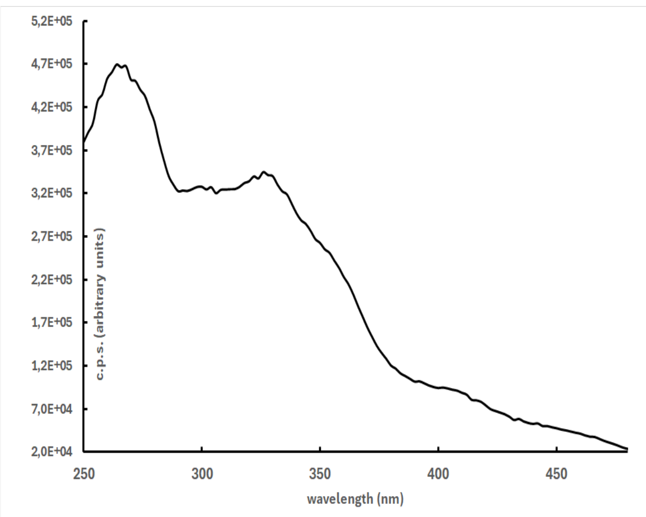

Excitation spectrum (λ_{max} = 566 nm), 298K

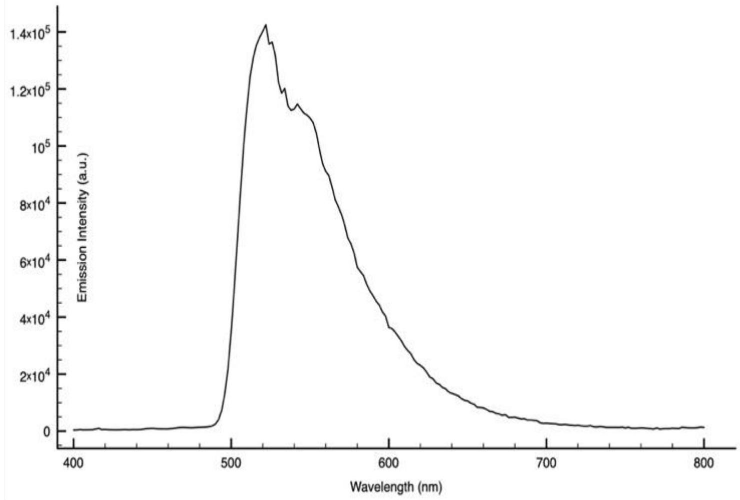

Emission profile, 77K

Figure S29: Photophysical Characterization of **[Ir(ppyCN)$_2$(PYZ-Me)]$^+$**, 10^{-5}M, CH_3CN.

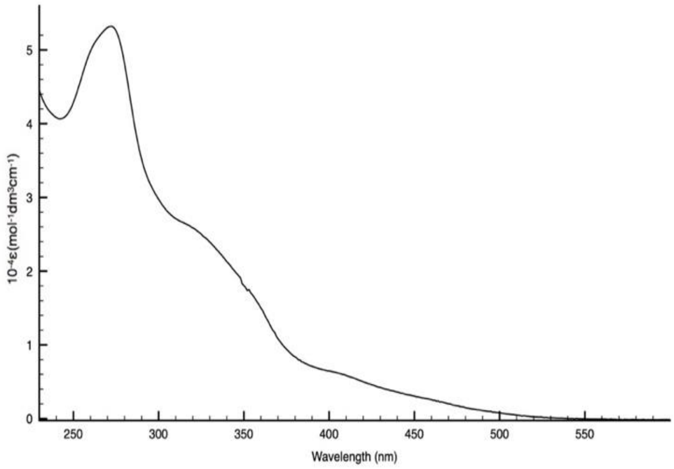

Absorption profile, 298K

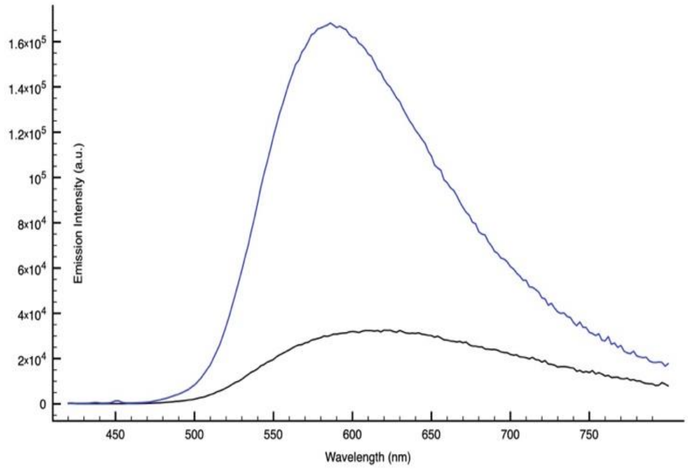

Air-equilibrated (black line) and deoxygenated (blue line) emission profiles, 298K

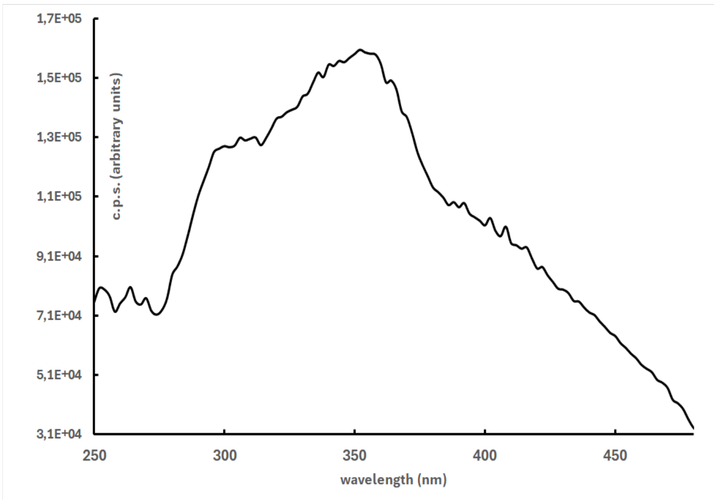

Excitation spectrum (λ_{max} = 614 nm), 298K

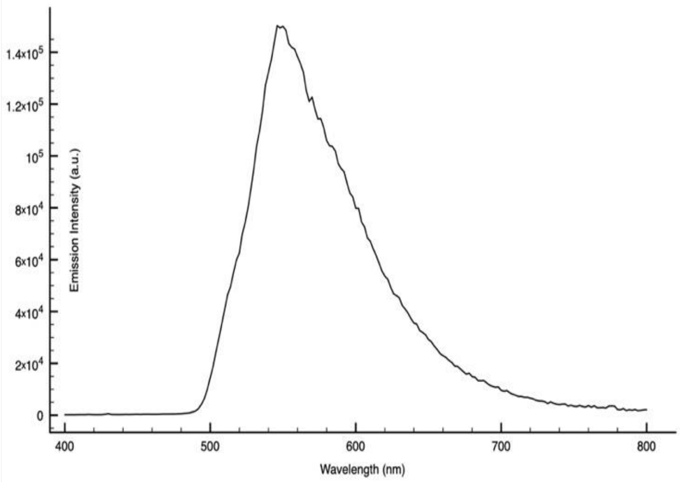

Emission profile, 77K

Figure S30: Photophysical Characterization of **[Ir(ppyCN)$_2$(PTZ-CF$_3$-Me)]$^+$**,10^{-5}M, CH_3CN.

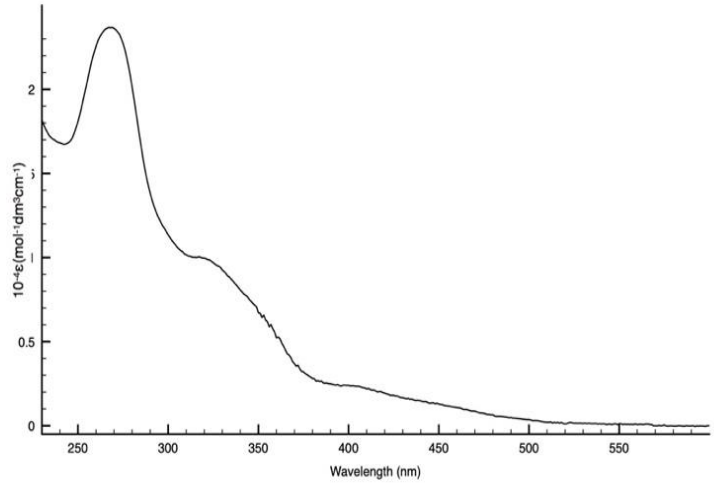

Absorption profile, 298K

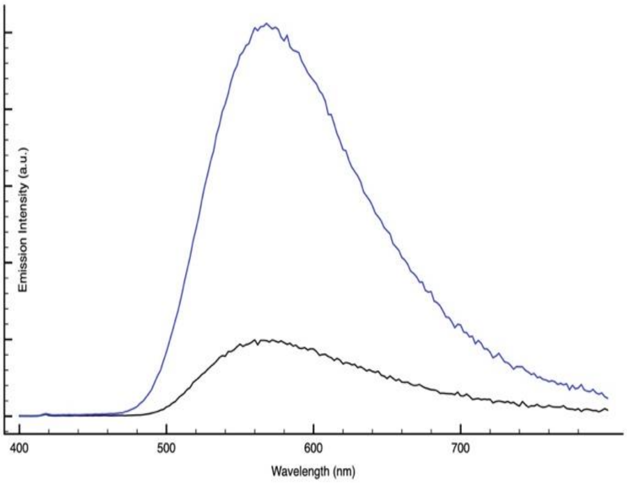

Air-equilibrated (black line) and deoxygenated (blue line) emission profiles, 298K

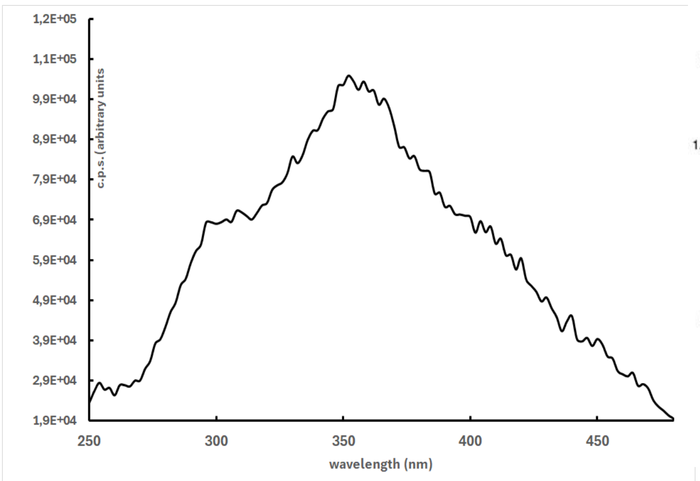

Excitation spectrum (λ_{max} = 568 nm), 298K

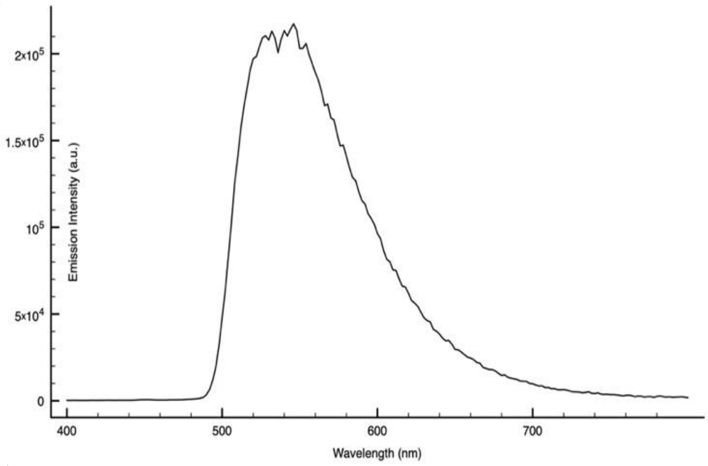

Emission profile, 77K

Figure S31: Photophysical Characterization of **[Ir(F_2ppy-CN)$_2$(PTZ)]**, 10^{-5}M, CH_3CN.

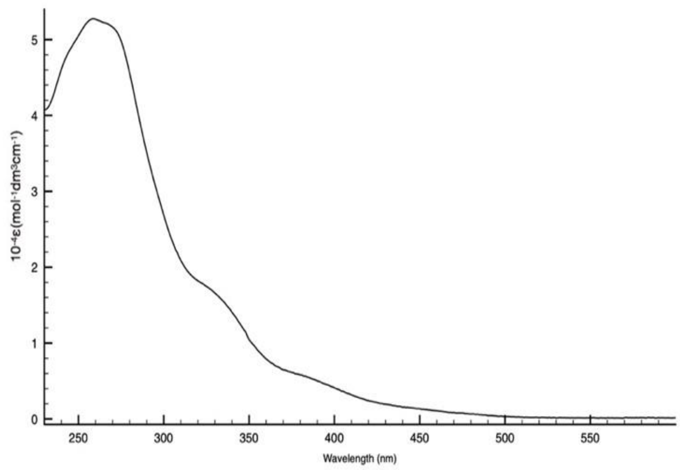

Absorption profile, 298K

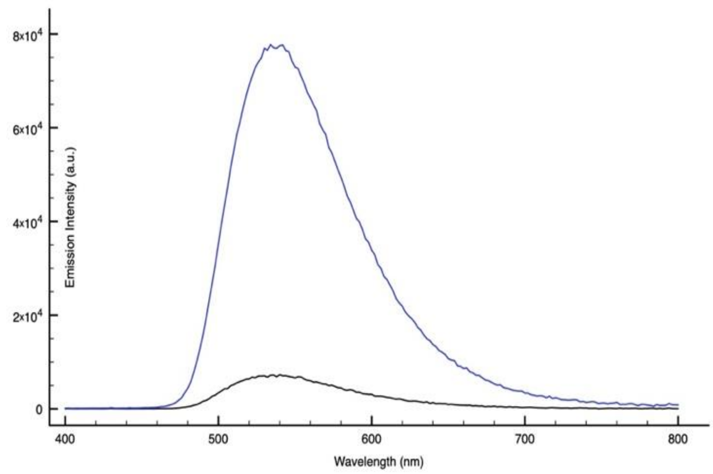

Air-equilibrated (black line) and deoxygenated (blue line) emission profiles, 298K

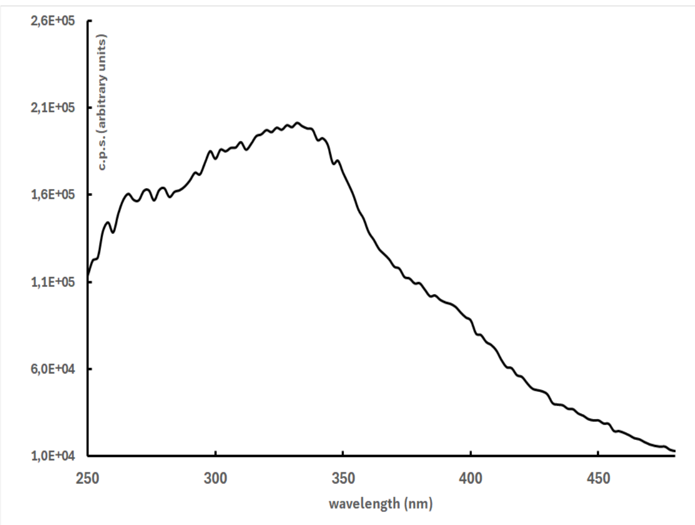

Excitation spectrum (λ_{max} = 540 nm), 298K

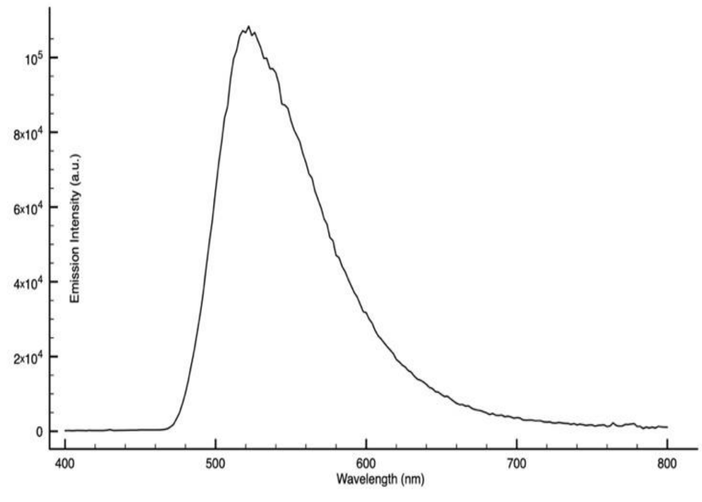

Emission profile, 77K

Figure S32: Photophysical Characterization of **[Ir(F_2ppy-CN)$_2$(PYZ)]**, 10^{-5}M, CH_3CN.

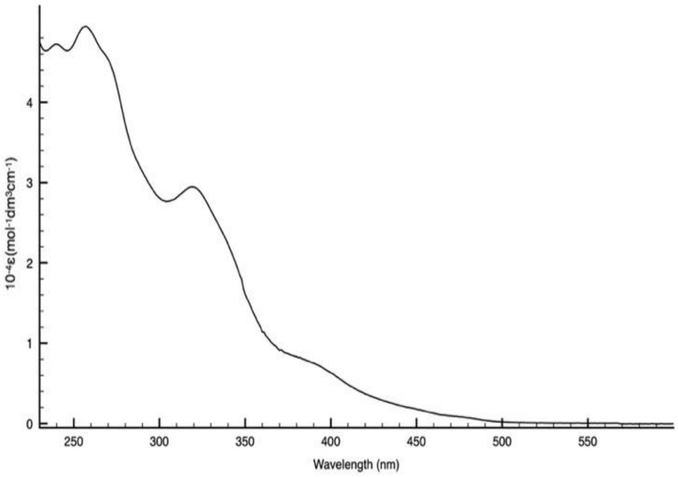

Absorption profile, 298K

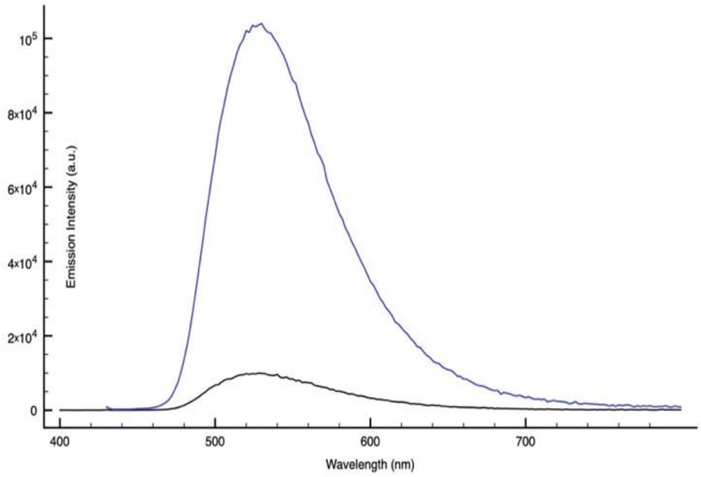

Air-equilibrated (black line) and deoxygenated (blue line) emission profiles, 298K

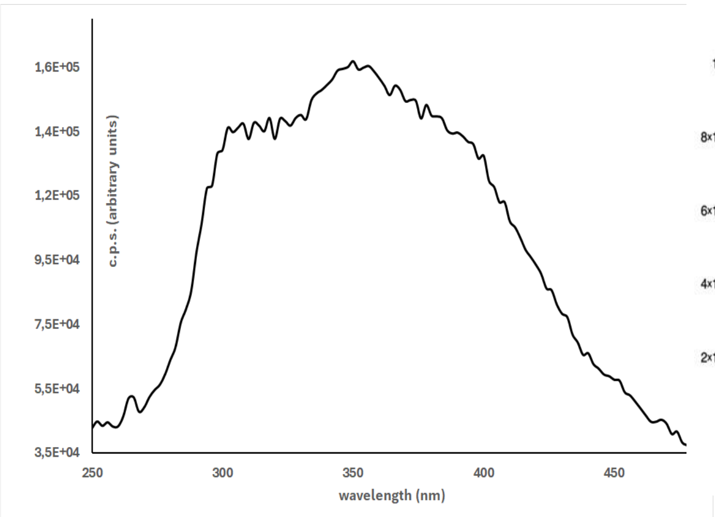

Excitation spectrum (λ_{max} = 532 nm), 298K

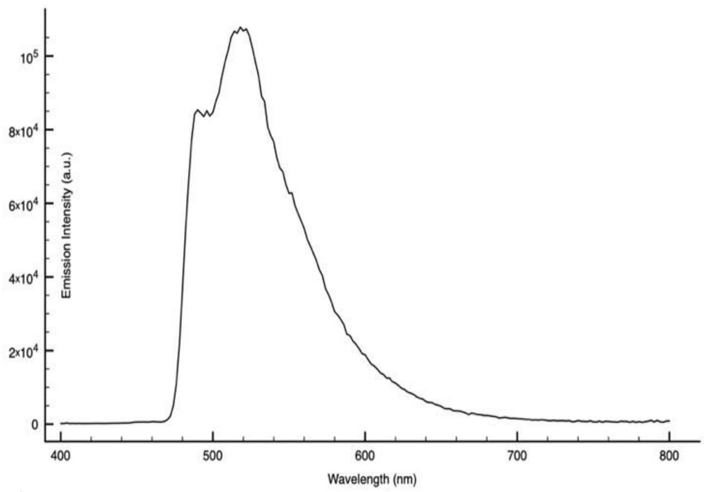

Emission profile, 77K

Figure S33: Photophysical Characterization of **[Ir(F$_2$ppy-CN)$_2$(PTZ-CF$_3$)]**, 10^{-5}M, CH_3CN.

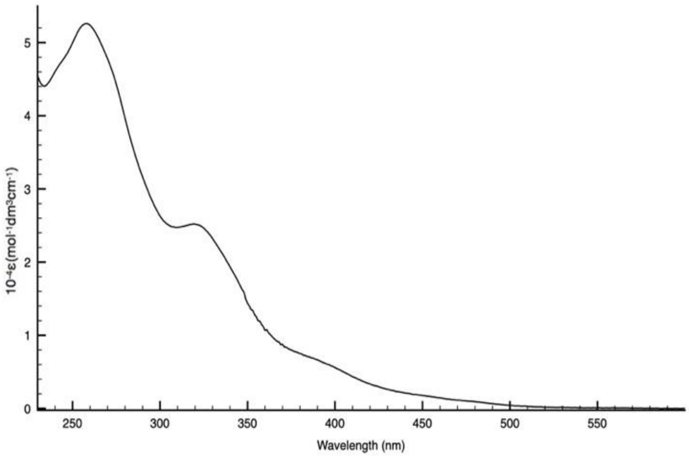

Absorption profile, 298K

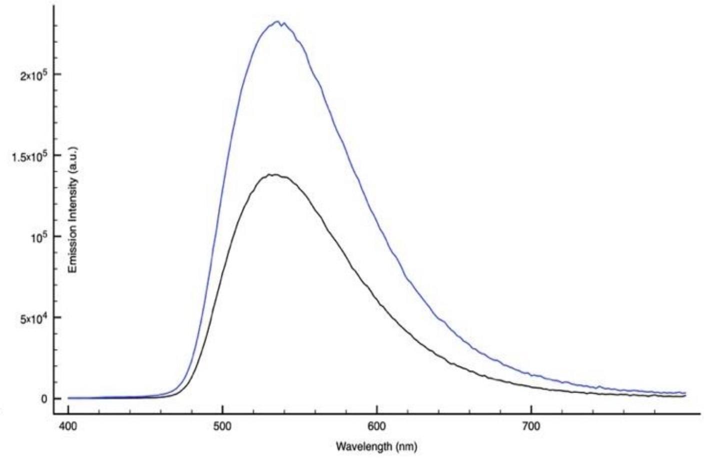

Air-equilibrated (black line) and deoxygenated (blue line) emission profiles, 298K

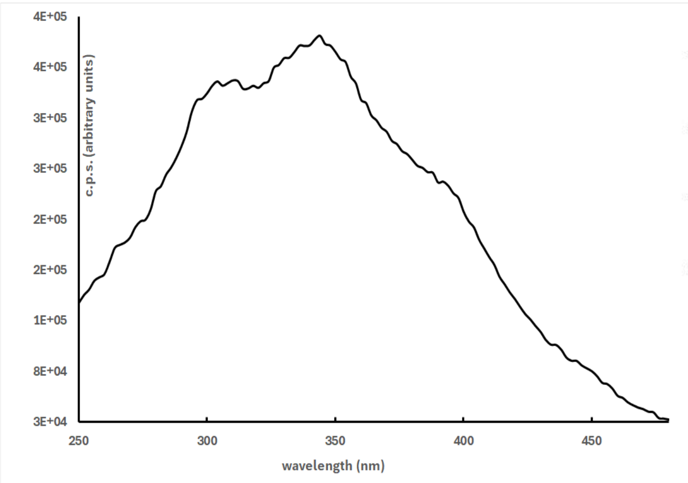

Excitation spectrum (λ_{max} = 536 nm), 298K

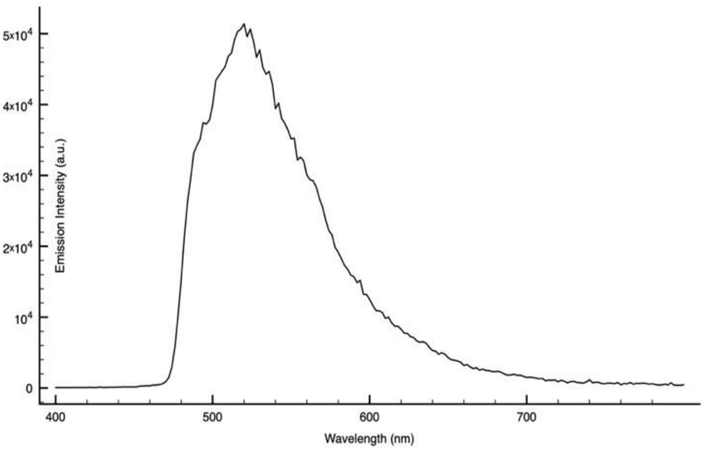

Emission profile, 77K

Figure S34: Photophysical Characterization of **[Ir(F$_2$ppy-CN)$_2$(PTZ-Me)]$^+$**, 10^{-5}M, CH_3CN.

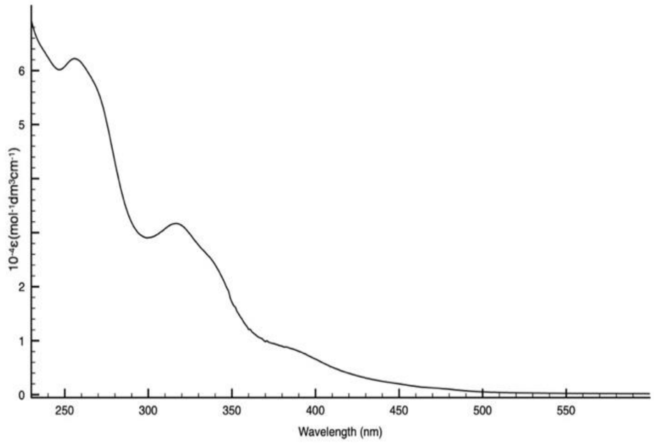

Absorption profile, 298K

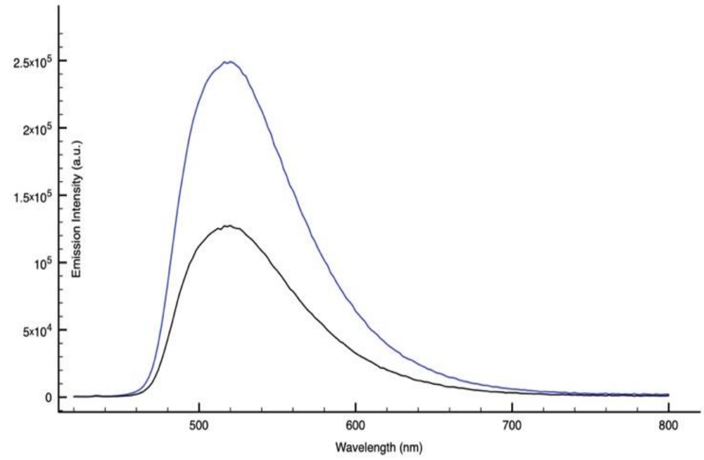

Air-equilibrated (black line) and deoxygenated (blue line) emission profiles, 298K

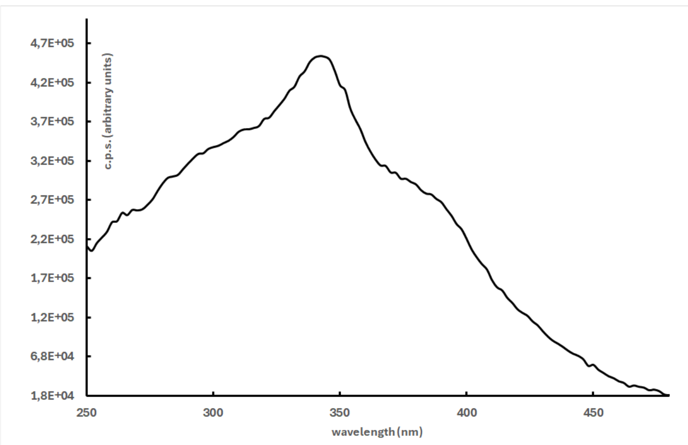

Excitation spectrum (λ_{max} = 520 nm), 298K

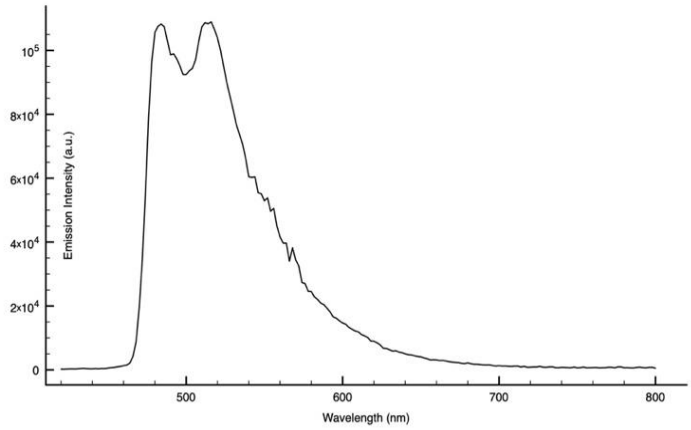

Emission profile, 77K

Figure S35: Photophysical Characterization of **[Ir(F_2ppy-CN)$_2$(PYZ-Me)]$^+$)]$^+$**, 10^{-5}M, CH_3CN.

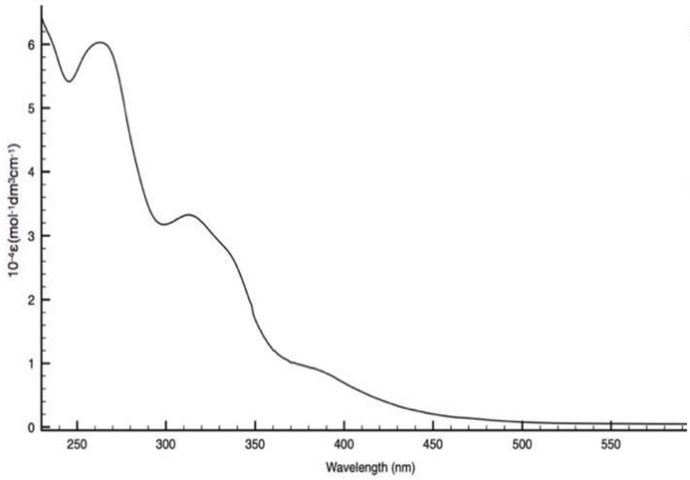

Absorption profile, 298K

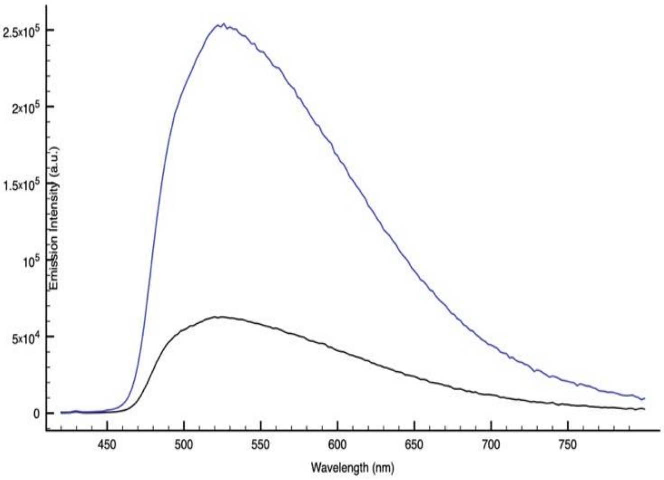

Air-equilibrated (black line) and deoxygenated (blue line) emission profiles, 298K

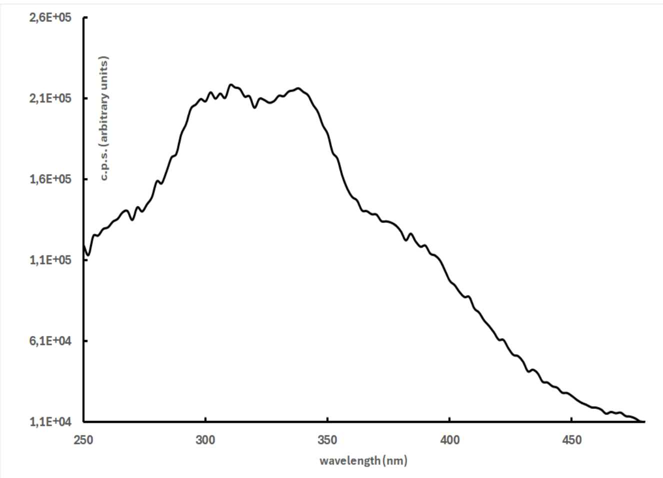

Excitation spectrum (λ_{max} = 530 nm), 298K

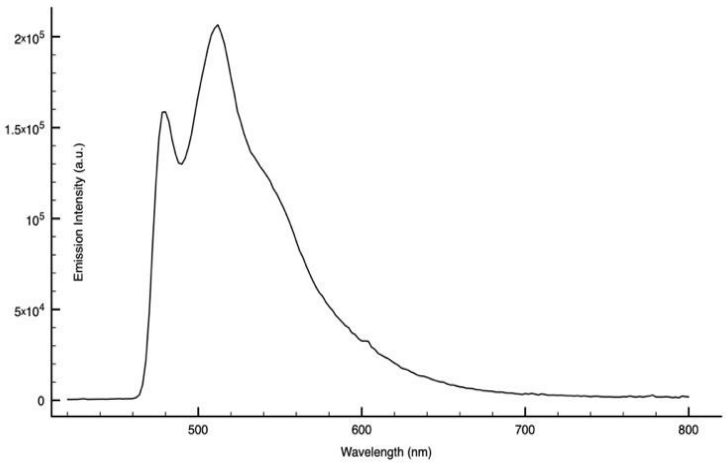

Emission profile, 77K

Figure S36: Photophysical Characterization of **[Ir(F_2ppy-CN)$_2$(PTZ-CF_3-Me)]$^+$**, 10^{-5}M, CH_3CN.

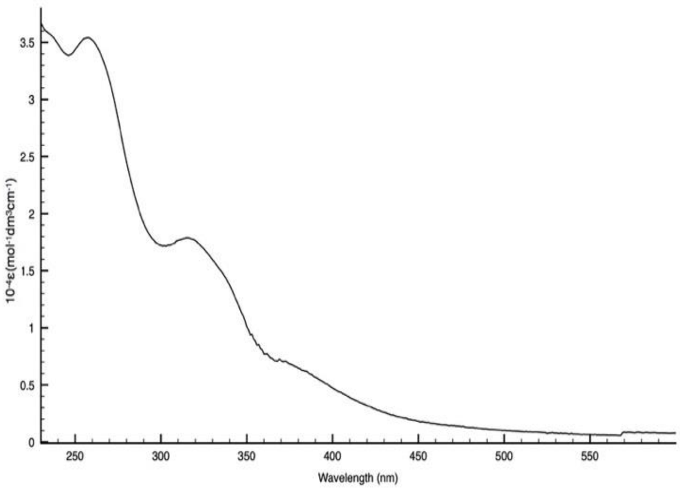

Absorption profile, 298K

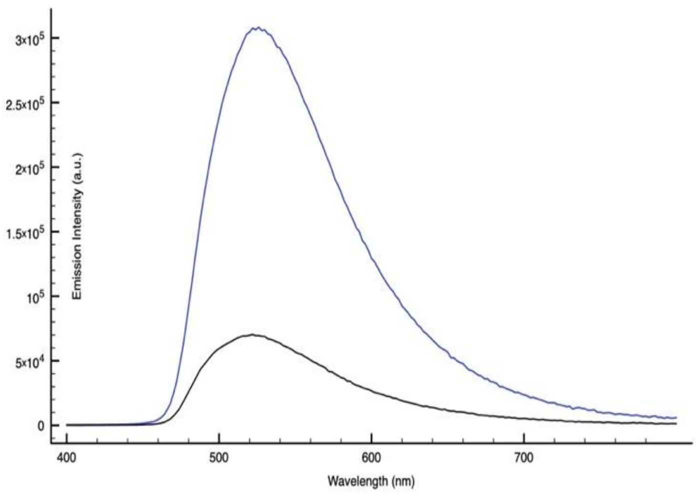

Air-equilibrated (black line) and deoxygenated (blue line) emission profiles, 298K

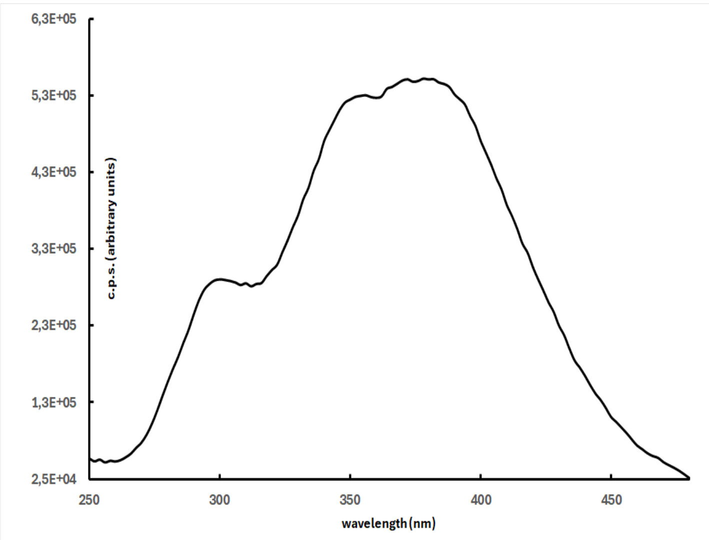

Excitation spectrum (λ_{max} = 520 nm), 298K

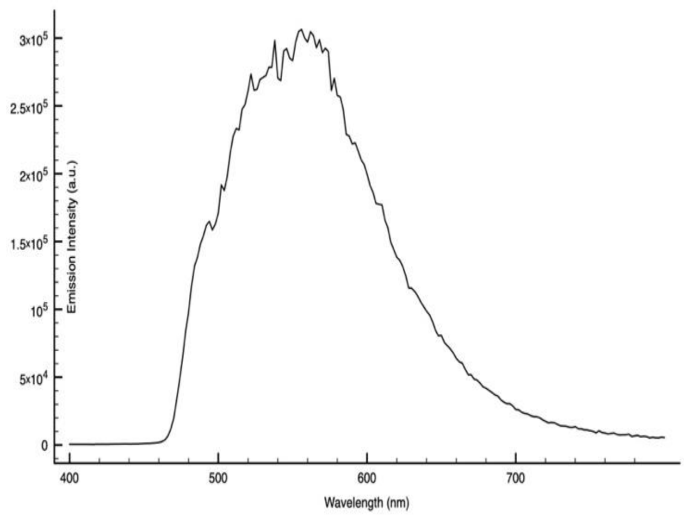

Emission profile, 77K

Figure S37: CV curves of **[Ir(ppyCN)$_2$(PYZ)]**, 10^{-3}M (a) oxidation, (b) reduction.

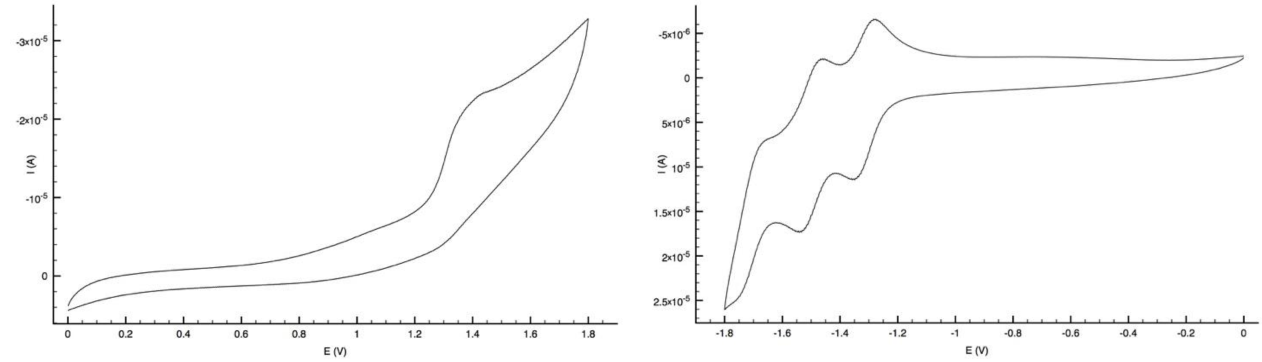

(a) (b)

Figure S38: CV curves of **[Ir(ppyCN)$_2$(PYZ-Me)]$^+$**, 10^{-3}M (a) oxidation, (b) reduction.

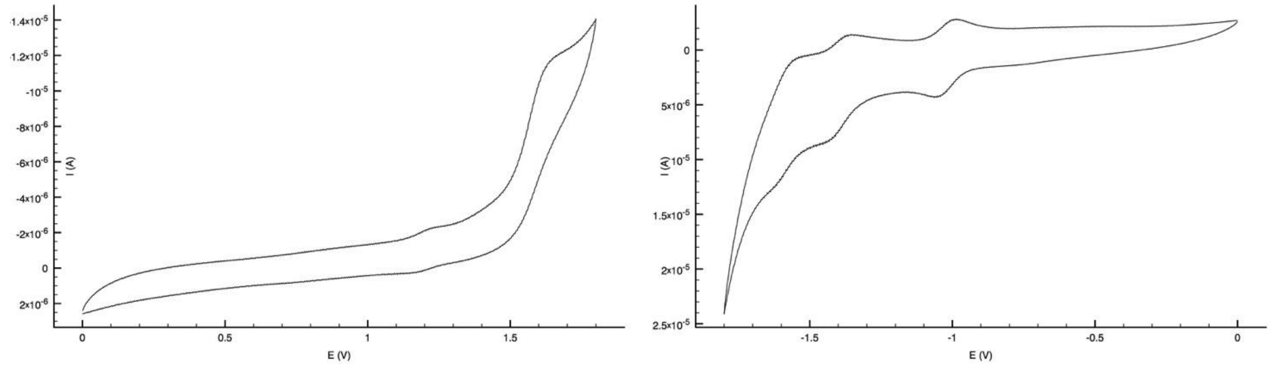

(a) (b)

Figure S39: CV curves of **[Ir(ppyCN)$_2$(PTZ)]**, 10^{-3}M (a) oxidation, (b) reduction.

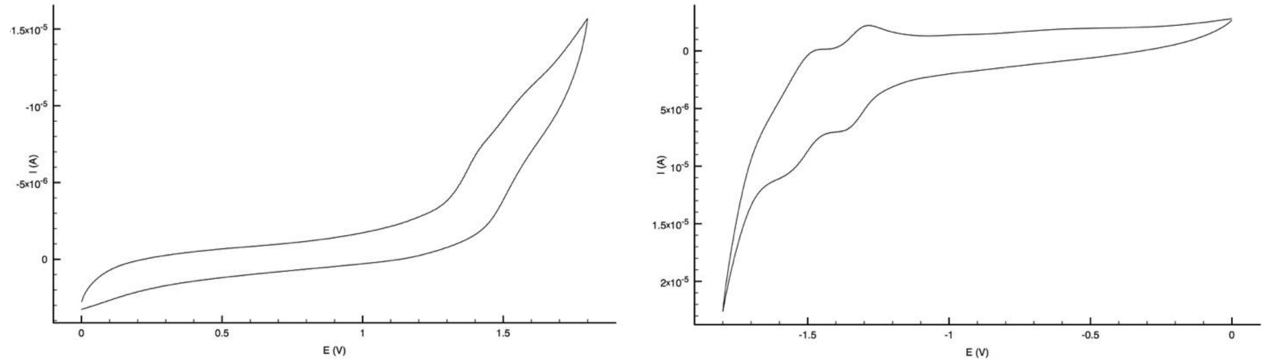

(a) (b)

Figure S40: CV curves of **[Ir(ppyCN)$_2$(PTZ-Me)]$^+$**, 10^{-3}M (a) oxidation, (b) reduction.

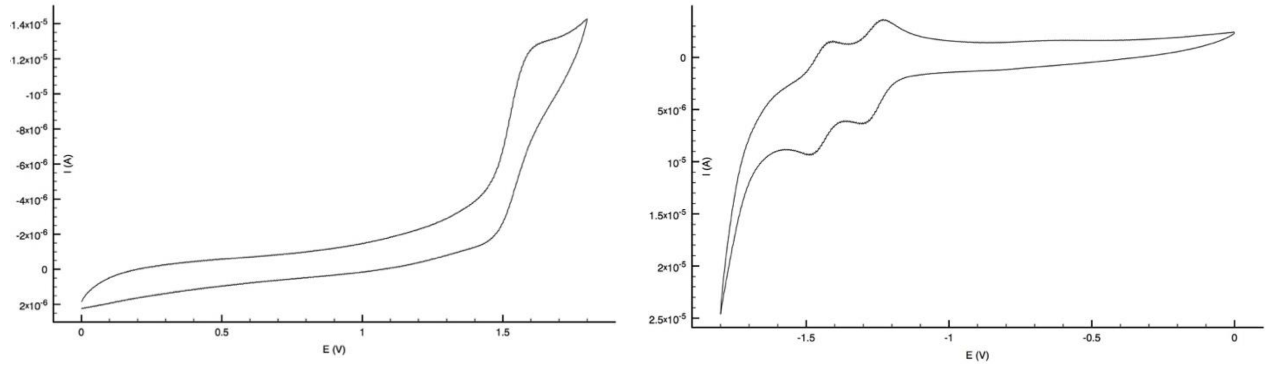

(a) (b)

Figure S41 CV curves of **[Ir(ppyCN)$_2$(PTZ-CF$_3$)]**, 10^{-3}M (a) oxidation, (b) reduction

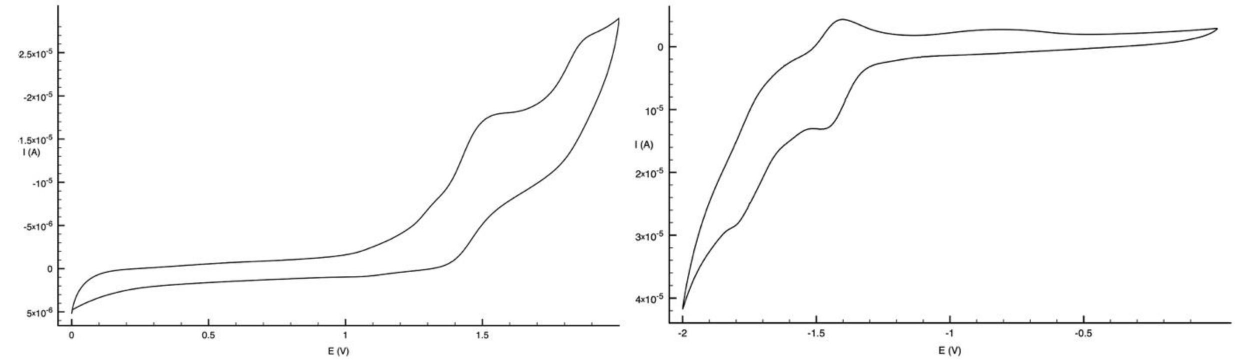

(a) (b)

Figure S42: CV curves of **[Ir(ppyCN)$_2$(PTZ-CF$_3$-Me)]$^+$**, 10^{-3}M (a) oxidation, (b) reduction.

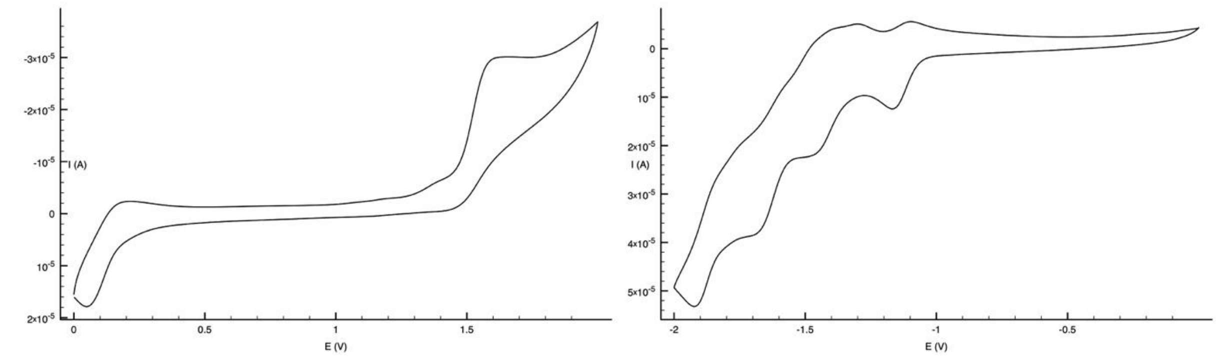

(a) (b)

Figure S43: CV curves of **[Ir(F$_2$ppy-CN)$_2$(PTZ)]**, 10^{-3}M (a) oxidation, (b) reduction.

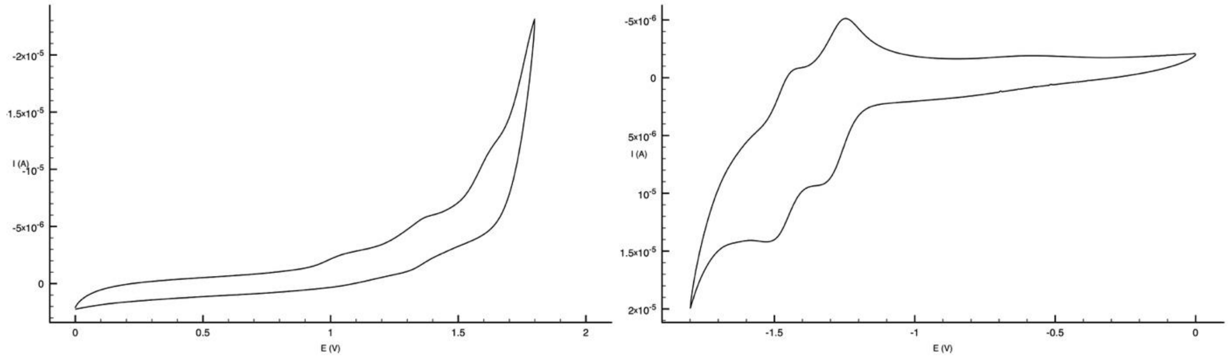

(a) (b)

Figure S44: CV curves of **[Ir(F$_2$ppy-CN)$_2$(PTZ)]**, 10^{-3}M (a) oxidation, (b) reduction.

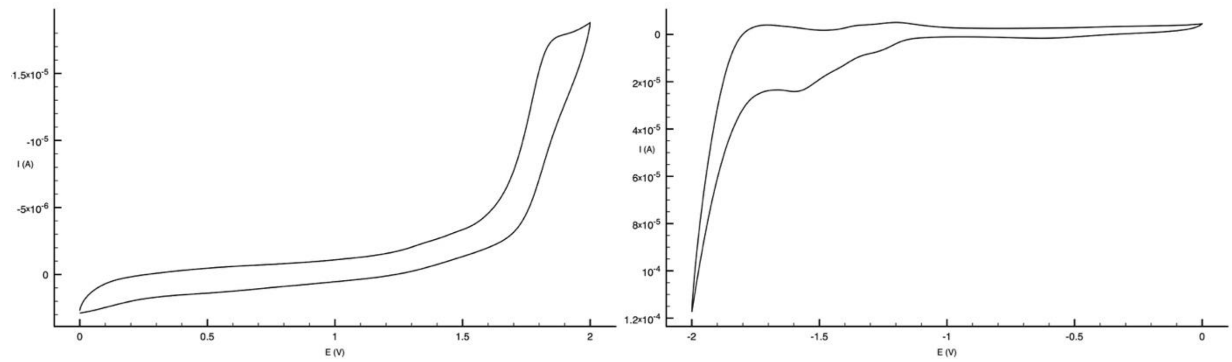

(a) (b)

Figure S45: CV curves of **[Ir(F_2ppy-CN)$_2$(PYZ)]**, 10^{-3}M (a) oxidation, (b) reduction.

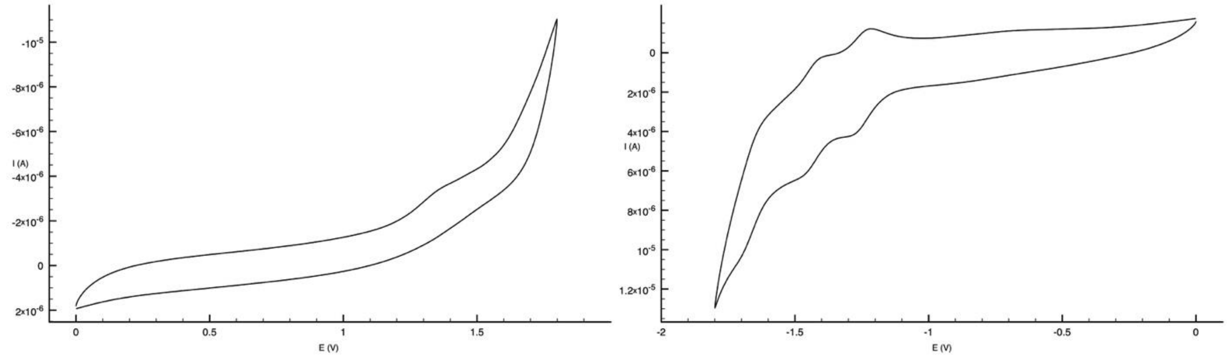

(a) (b)

Figure 46: CV curves of **[Ir(F_2ppy-CN)$_2$(PYZ-Me)]$^+$**, 10^{-3}M (a) oxidation, (b) reduction.

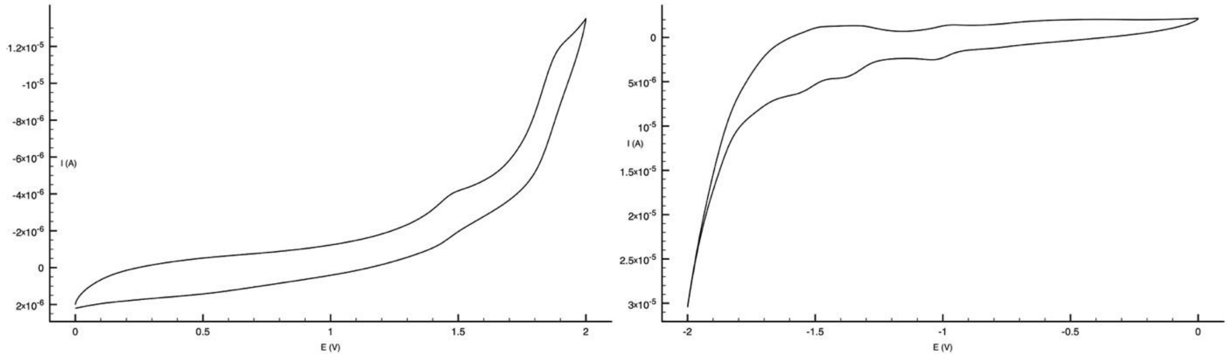

(a) (b)

Figure S47: CV curves of **[Ir(F_2ppy-CN)$_2$(PTZ-CF_3)]**, 10^{-3}M (a) oxidation, (b) reduction.

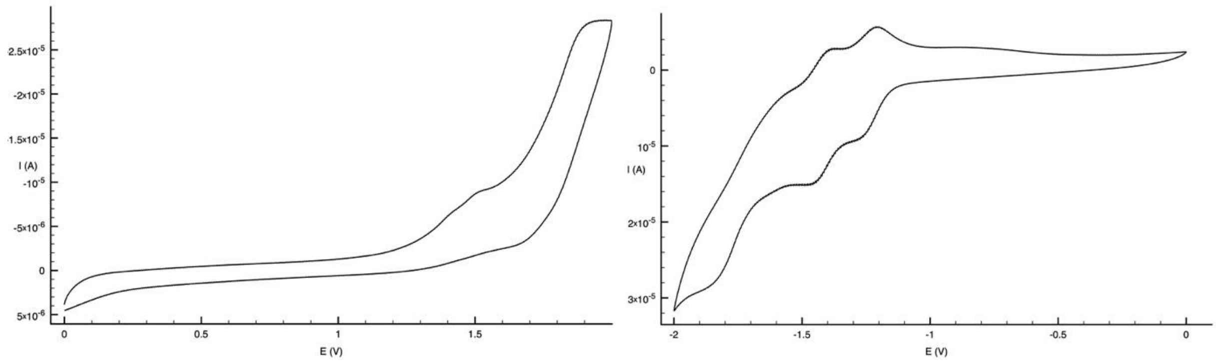

(a) (b)

Figure S48: CV curves of **[Ir(F_2ppy-CN)$_2$(PTZ-CF_3-Me)]$^+$**, 10^{-3}M (a) oxidation, (b) reduction.

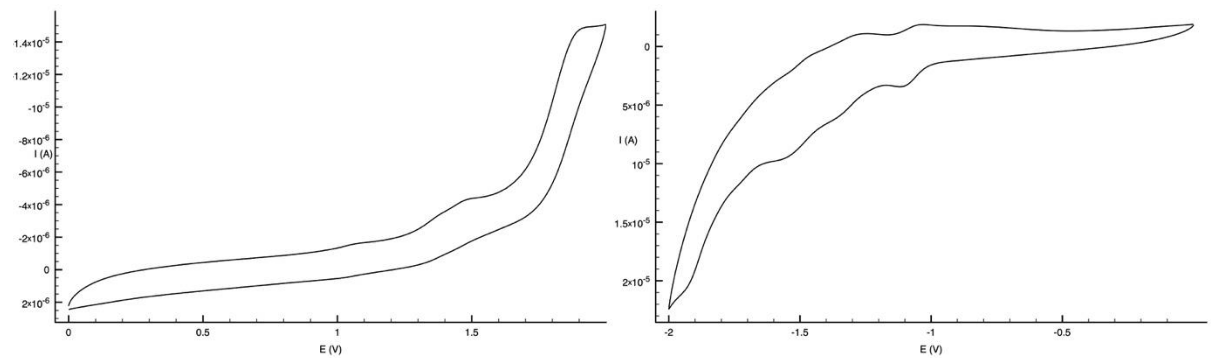

(a) (b)

Tentative photostability test on **[Ir(F2ppy-CN)2(PTZ)]**

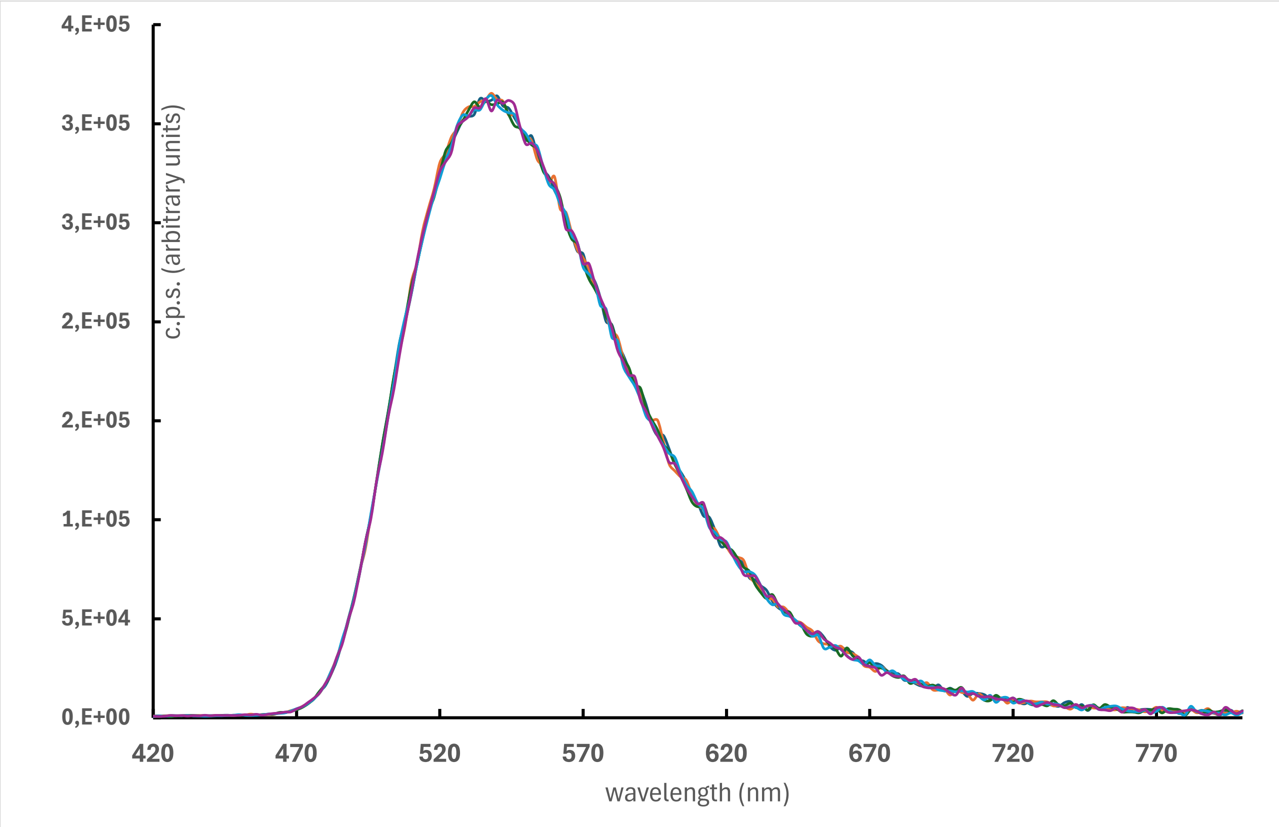

Figure S49. Five successive emission profiles recorded after successive cycle of irradiation (20 min. exposure, Xe arc lamp 450W, λexc = 350 nm, slit = 5 nm).

X-ray crystallography

Table S1: Crystal data and collection details for **[Ir(ppyCN)$_2$(PTZ-CF$_3$)]·solv**.

Formula	$C_{31}H_{17}F_3IrN_9$
Fw	764.73
T, K	100(2)
λ, Å	0.71073
Crystal system	Monoclinic
Space Group	$P2_1/c$
a, Å	12.1158(13)
b, Å	14.7808(16)
c, Å	20.394(2)
β, °	105.660(3)
Cell Volume, Å^3	3516.6(7)
Z	4
D_c, g cm^{-3}	1.444
μ, mm^{-1}	3.844
F(000)	1480
Crystal size, mm	0.16×0.15×0.12
θ limits, °	1.724–24.998
Index ranges	$-14 \leq h \leq 14$ $-17 \leq k \leq 17$ $-24 \leq l \leq 24$
Reflections collected	29645
Independent reflections	6116 [R_{int} = 0.1061]
Completeness to θ max	98.7%
Data / restraints / parameters	6116 / 300 / 397
Goodness on fit on F^2	1.245
R_1 ($I > 2\sigma(I)$)	0.1300
wR_2 (all data)	0.2943
Largest diff. peak and hole, e Å^{-3}	4.172 / –1.640

TD-DFT

Table S2: Contour HOMO – LUMO for all the neutral and cationic fluorine-free Ir(III) compounds. from left to right: **[Ir(ppyCN)$_2$(PTZ)]**, **[Ir(ppyCN)$_2$(PTZ-Me)]$^+$**, **[Ir(ppyCN)$_2$(PYZ)]**, **[Ir(ppyCN)$_2$(PYZ-Me)]$^+$**, **[Ir(ppyCN)$_2$(PTZ-CF$_3$)]**, **[Ir(ppyCN)$_2$(PTZ-CF$_3$-Me)]$^+$**. The images were produced using the Gaussian outputs, but the results are analogous to those obtained from ORCA

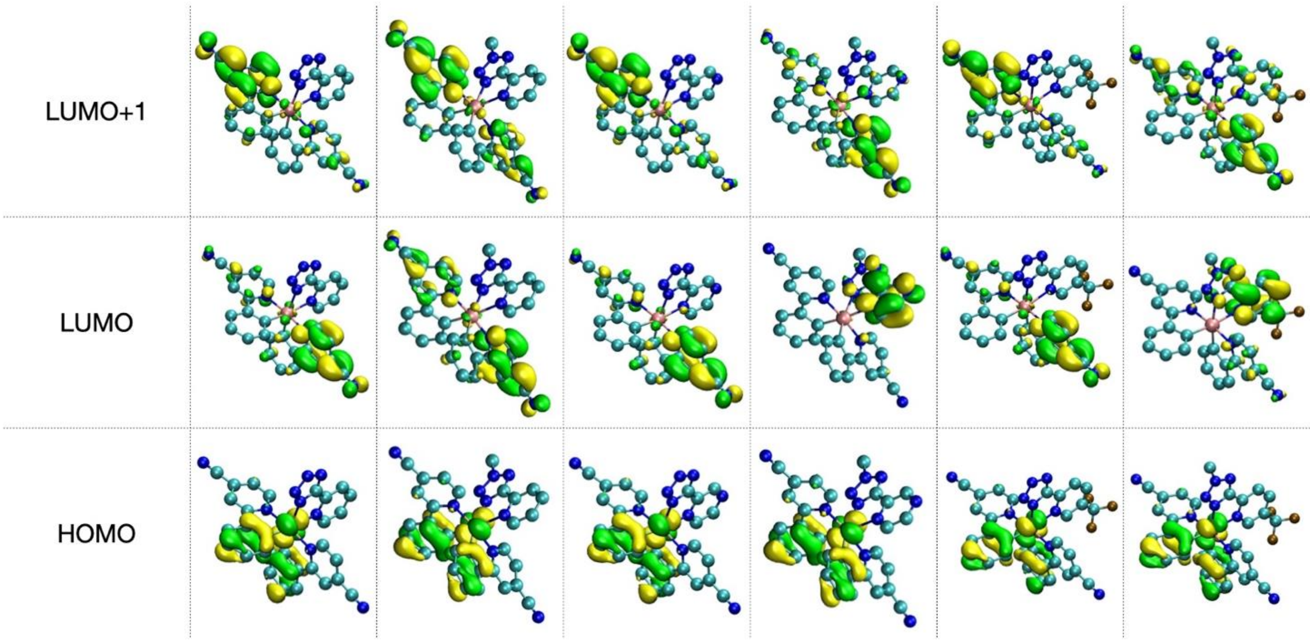

Table S3: Contour HOMO – LUMO for all the neutral and cationic fluorinated Ir(III) compounds. from left to right: **[Ir(F_2ppy-CN)$_2$(PTZ)]**, **[Ir(F_2ppy-CN)$_2$(PTZ-Me)]$^+$**, **[Ir(F_2ppy-CN)$_2$(PYZ)]**, **[Ir(F_2ppy-CN)$_2$(PYZ-Me)]$^+$**, **[Ir(F_2ppy-CN)$_2$(PTZ-CF_3)]**, **[Ir(F_2ppy-CN)$_2$(PTZ-CF_3-Me)]$^+$**. The images were produced using the Gaussian outputs, but the results are analogous to those obtained from ORCA

LUMO+1	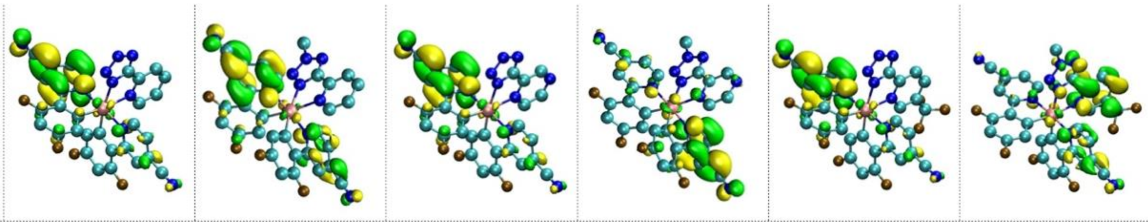
LUMO	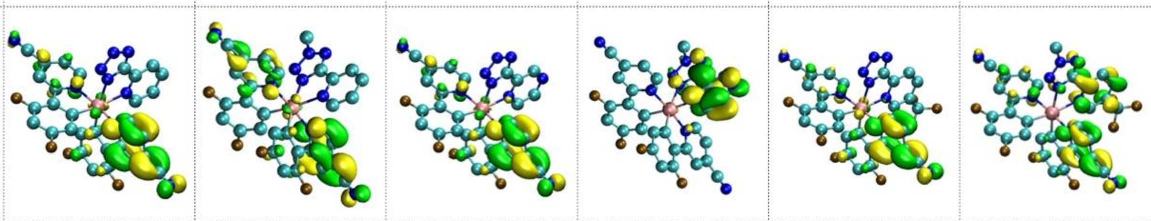
HOMO